Journal of South American Earth Sciences 133 (2024) 104696

Contents lists available at ScienceDirect

Journal of South American Earth Sciences

journal homepage: www.elsevier.com/locate/jsames

New advances on the carbon isotope and rare earth elements chemostratigraphy of the late Ediacaran Tamengo Formation (Corumbá Group, Brazil)

Henrique Albuquerque Fernandes [a,*], Paulo César Boggiani [a], Aghata Zarelli Viana [b], Sergio Caetano-Filho [c], Luiz Gustavo Pereira [a], Bernardo Tavares Freitas [d], João Pedro Hippertt [e], Luana Morais [c,f], Ricardo Ivan Ferreira Trindade [f]

[a] Instituto de Geociências, Universidade de São Paulo, São Paulo, SP, Brazil
[b] Faculté de Sciences Appliquées, Université de Liège, Liège, Belgium
[c] Departamento de Geologia, Universidade Estadual Paulista, Rio Claro, SP, Brazil
[d] Universidade Estadual de Campinas (UNICAMP), Faculdade de Tecnologia, Limeira, SP, Brazil
[e] Departamento de Geologia, Universidade Federal de Ouro Preto, Ouro Preto, MG, Brazil
[f] Instituto de Astronomia, Geofísica e Ciências Atmosféricas, Universidade de São Paulo, São Paulo, SP, Brazil

ARTICLE INFO

Keywords:
Corumbá Group
Tamengo Formation
Carbon isotopes
Rare earth elements
Chemostratigraphy

ABSTRACT

The Tamengo Formation (Corumbá Group, midwest Brazil) is a carbonate-dominated succession of major importance to unravel the environmental and biological changes during the Ediacaran–Cambrian transition in Gondwana. Although it has been extensively studied in terms of sedimentology, isotope geochemistry, biostratigraphy, and geochronology, these studies are constrained to the Corumbá region. This work presents new sedimentological, C and O isotope chemostratigraphy, and rare earth elements (REE) plus yttrium (REY) data of four sections of the Tamengo Formation in the Serra da Bodoquena region, approximately 200 km south of Corumbá, discussing how these new data are related to the type sections. The sections present ooid grainstones, with hummocky, swaley, and wavy structures, interbedded with mudstones and shales, indicating deposition of fine particles by suspension fallout in-between periods of high-energy, with reworking by storm waves. The $\delta^{13}C_{carb}$ curves show positive plateaus with minor, short-lived negative excursions linked to facies variations, which are related to a large $\delta^{13}C_{carb}$ depth gradient in a redox-stratified water column. The REY profiles present middle REE (MREE)-bulge patterns and absent to slightly positive Ce anomalies, consistent with MREE adsorption onto Fe–Mn oxyhydroxides in the water column followed by release in pore waters. Subsequently, REY remobilization during anoxic diagenetic stages resulted in the MREE-bulge pattern and overprinted some of the original seawater REY features, including the Ce anomalies. The Tamengo Formation in the Serra da Bodoquena region represents a storm-dominated carbonate ramp, as previously interpreted for this unit in the Corumbá region. Nevertheless, there is a significant shift of 2 ‰ in the peaks of $\delta^{13}C_{carb}$ data between both localities, which may be related to differences in the overall sector of the carbonate ramp. There are also substantial variations in the $\delta^{13}C_{carb}$ record of the Tamengo Formation and other coeval Gondwana basins, such as the Nama and Itapucumi groups, with different peak values, which may be related to latitudinal differences on the inorganic carbon isotope composition or to the degree of basin restriction.

1. Introduction

The Ediacaran–Cambrian boundary is one of the most intriguing transitions in the geological record. It encompasses metazoan radiations (Droser et al., 2017; Wood et al., 2019), dramatic fluctuations in atmosphere-ocean redox conditions (Bowyer et al., 2017; Frei et al., 2013; Mills and Canfield, 2014; Och and Shields-Zhou, 2012; Sahoo et al., 2016; Tostevin et al., 2016b), and major disturbances in the global carbon cycle (Bjerrum and Canfield, 2011; Bowyer et al., 2022; Johnston et al., 2012; Rothman et al., 2003; Yang et al., 2021). To investigate such

* Corresponding author.
E-mail address: henriqueaf@usp.br (H.A. Fernandes).

https://doi.org/10.1016/j.jsames.2023.104696
Received 29 May 2023; Received in revised form 16 October 2023; Accepted 14 November 2023
Available online 21 November 2023

processes, a few Ediacaran sedimentary units have been extensively studied over the past decades. However, an integrated approach, considering combined studies of several Ediacaran units worldwide, is also a powerful way to explore both environmental and biological innovations (e.g., Boddy et al., 2022). The Gondwana basins, in particular, recorded the influence of tectonic movements in the Ediacaran–Cambrian ecosystems and their consequence on the rise of complex life (Caxito et al., 2021; Cordani et al., 2020).

Stable carbon isotopes have been one of the most used tools in paleoenvironmental studies during the past decades. This is due to the relatively fast acquisition time, simple sample preparation, relatively low cost of analysis, and the relatively good understanding of the carbon cycle built over the years (Caxito et al., 2019). The canonical interpretation of the carbon isotope signature of carbonate rocks is that the $\delta^{13}C_{carb}$ signal varies according to the global carbon cycle (Hayes et al., 1999). However, other factors unrelated to global-scale processes may play an even more critical role in determining the $\delta^{13}C_{carb}$ signal of a carbonate rock. For example, diagenesis may overprint the C and O isotope signature through basin fluid percolation (Banner and Hanson, 1990; Jacobsen and Kaufman, 1999). Likewise, isotope fractionation linked to authigenic carbonate precipitation may also explain some of the $\delta^{13}C_{carb}$ excursions throughout the geological record (Laakso and Schrag, 2020). Therefore, both global and local drivers may influence the $\delta^{13}C_{carb}$ record of a carbonate succession.

Furthermore, rare earth elements (REE) in carbonates may be used to track variations in past seawater chemistry (Tostevin et al., 2016a). In the modern seawater, rare earth elements and yttrium (REY) commonly present the so-called "seawater signal", with positive La anomaly, negative Ce anomaly, minor positive Gd anomaly, light REE (LREE) depletion, and Y/Ho ratios above chondritic values (Nozaki et al., 1997; Zhang and Nozaki, 1996). Carbonates that present a seawater-like REY signature are often considered to preserve the original seawater composition. Nevertheless, it is common for ancient carbonates to display different patterns, including middle REE (MREE)-bulge, heavy REE (HREE)-depleted, and flat profiles (Zhao et al., 2021, 2022). In those cases, the carbonate REY signature records either post-depositional processes responsible for REY remobilization and overprint or variations in the seawater REY distribution, demanding a careful investigation.

The carbonate-dominated Tamengo Formation (Corumbá Group, midwest Brazil) is a key unit to investigate metazoan radiations and geochemical variations in Southwestern Gondwana during the Ediacaran–Cambrian boundary. This relevance comes from its rich paleontological content, with skeletonized fossils (Adorno et al., 2017; Becker-Kerber et al., 2017; Hahn et al., 1982; Hahn and Pflug, 1985; Walde et al., 2015; Zaine and Fairchild, 1985, 1987), fossils of macroalgae (Diniz et al., 2021), acritarchs (Gaucher et al., 2003; Zaine, 1991), conulariids (Leme et al., 2022), vendotaenids (Becker-Kerber et al., 2022) and ichnofossils of meiofaunal bilaterians (Parry et al., 2017) linked to well preserved geochemical signatures, as revealed from studies of carbon stable isotopes (Boggiani et al., 2010; Ramos et al., 2022), nitrogen isotopes (Oliveira et al., 2019), and major and trace elements chemostratigraphy (Spangenberg et al., 2014). Nearly all the investigations on the Tamengo Formation were based on the type sections in the Corumbá region, mainly the Laginha and Corcal quarries. However, the Tamengo Formation also crops out broadly in the Serra da Bodoquena region, approximately 200 km south of Corumbá.

The purpose of this paper is to present novel sedimentological, isotope and rare earth elements data of the Tamengo Formation in the Serra da Bodoquena region, discussing the depositional setting of the Tamengo Formation in this area, the influence of anoxic diagenesis in the REY geochemistry, the implications of seawater redox stratification to the carbon isotope record, and the correlation of this unit with the Corumbá area and other Late Ediacaran Gondwana basins.

2. Geological setting

The Paraguay Belt is a Neoproterozoic to Early Cambrian fold-thrust belt that originated during the collision of Amazonia/Rio Apa and Paranapanema cratons by the end of the Brasiliano Orogeny (Trompette, 1994). It is divided into the northern and southern branches (Fig. 1), which have significant differences in stratigraphy and geochronology (Alvarenga et al., 2010; Babinski et al., 2013). The southern Paraguay Belt comprises sedimentary and metasedimentary rocks of the Puga Formation, Corumbá Group, and Jacadigo Group (Almeida, 1965; Alvarenga et al., 2010; Boggiani, 1998; Freitas et al., 2011, 2021), metamorphic rocks attributed to the Cuiabá and Rio Bacuri groups (Campanha et al., 2011), and igneous plutonic rocks, essentially post-collisional granitoids (Manzano et al., 2008). In general, the intensity of deformation increases from west to east (Alvarenga and Trompette, 1993; Campanha et al., 2011; D'el-Rey Silva et al., 2016; Trompette et al., 1998). In the southern Paraguay Belt, there are two major studied areas where the Precambrian rocks are not covered by Cenozoic sediments, the Corumbá surroundings to the north and the Serra da Bodoquena region to the south, both ca. 200 km apart (Fig. 1).

The Puga Formation is the only sedimentary unit recognized in both northern and southern branches of the Paraguay Belt. It comprises diamictites interbedded with conglomerates, sandstones, and shales (Almeida, 1965; Boggiani, 1998; Boggiani et al., 2003), presenting facies of platformal, slope, and outer slope depositional settings (Alvarenga and Trompette, 1993). The Puga Formation was first described in the southern Paraguay Belt, specifically at the Puga Hill (Maciel, 1959), where it is sharply overlain by a distinct cap carbonate, with tubestone-microbialite facies and negative $\delta^{13}C_{carb}$ values (Boggiani et al., 2003; Romero et al., 2016). In the northern Paraguay Belt, the Puga cap carbonate, represented by the Mirassol D'Oeste and Guia formations, presents typical post-Marinoan cap carbonate characteristics such as tubestone-microbialite association, megaripples, and megapelloids (Font et al., 2006; Nogueira et al., 2003, 2022). In the southern Paraguay Belt, detrital zircon ages constrain the maximum depositional age of the Puga Formation at 686 ± 10 Ma (McGee et al., 2018), ruling out any correlation of this unit with the Sturtian Glaciation. The Puga Formation is associated with the upper Jacadigo Group due to the extensive banded iron formations found in both units (Alvarenga et al., 2011), their interpreted glacial origin (Freitas et al., 2021), and their correlative Cr isotope chemostratigraphy (Árting et al., 2023; Frei et al., 2017). Furthermore, recent *in situ* U–Pb dating of calcite in the Puga cap carbonate in the northern Paraguay Belt yielded an age of 623 ± 3 Ma, interpreted as diagenetic stabilization of the cap carbonate fabric (Carvalho et al., 2023). Considering the points listed above, an end-Cryogenian (Marinoan) age for the Puga Formation and an earliest Ediacaran age (ca. 635 Ma) for the overlying cap carbonate are more consistent with the available data.

The Corumbá Group unconformably overlies the Puga Formation and the Puga cap dolostone, encompassing Ediacaran siliciclastic and carbonate rocks divided into Cadiueus, Cerradinho, Bocaina, Tamengo, and Guaicurus formations, from base to top (Almeida, 1965; Boggiani, 1998). The Cadiueus Formation marks the initial stages of sedimentation as conglomerates with basement clasts, representing glacial-outwash fans and gradually passing to facies of the Cerradinho Formation (Almeida, 1965; Boggiani, 1998; Gaucher et al., 2003). The Cerradinho Formation hosts thick beds of sandstones interbedded with carbonates and shales, representing the upper facies of the fans (Almeida, 1965; Alvarenga et al., 2010; Boggiani, 1998). These two basal units (Cadiueus and Cerradinho formations) represent the initial rift stage of the Corumbá Basin, with predominantly terrigenous input into grabens (Boggiani et al., 2010). The microfossil assemblage of the Cerradinho Formation supports an Ediacaran age for this unit (Gaucher et al., 2003), but Hiatt et al. (2020) advocates an end-Cryogenian age for the Cadiueus and Cerradinho formations based on glacial sedimentary features of drill cores from the Corumbá area, associating them with the Marinoan

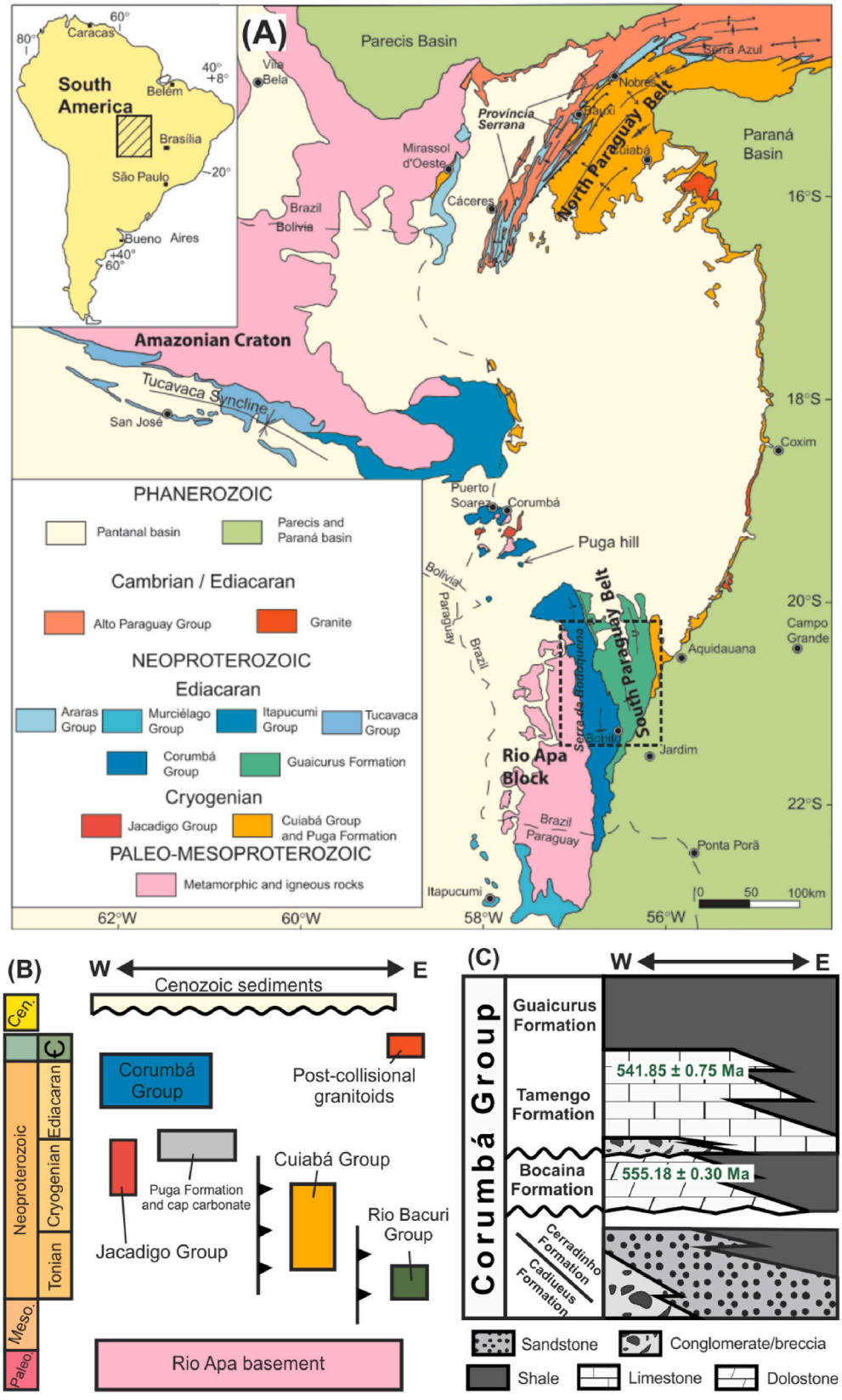

Fig. 1. (A) Geological map of the Paraguay Belt and associated units (after Alvarenga et al., 2010). The dashed rectangle denotes the area of the geological map of Fig. 2. (B) Stratigraphic chart of the southern Paraguay Belt. (C) Stratigraphic chart of the Corumbá Group. Green ages are U–Pb ash bed zircon ages from Parry et al. (2017).

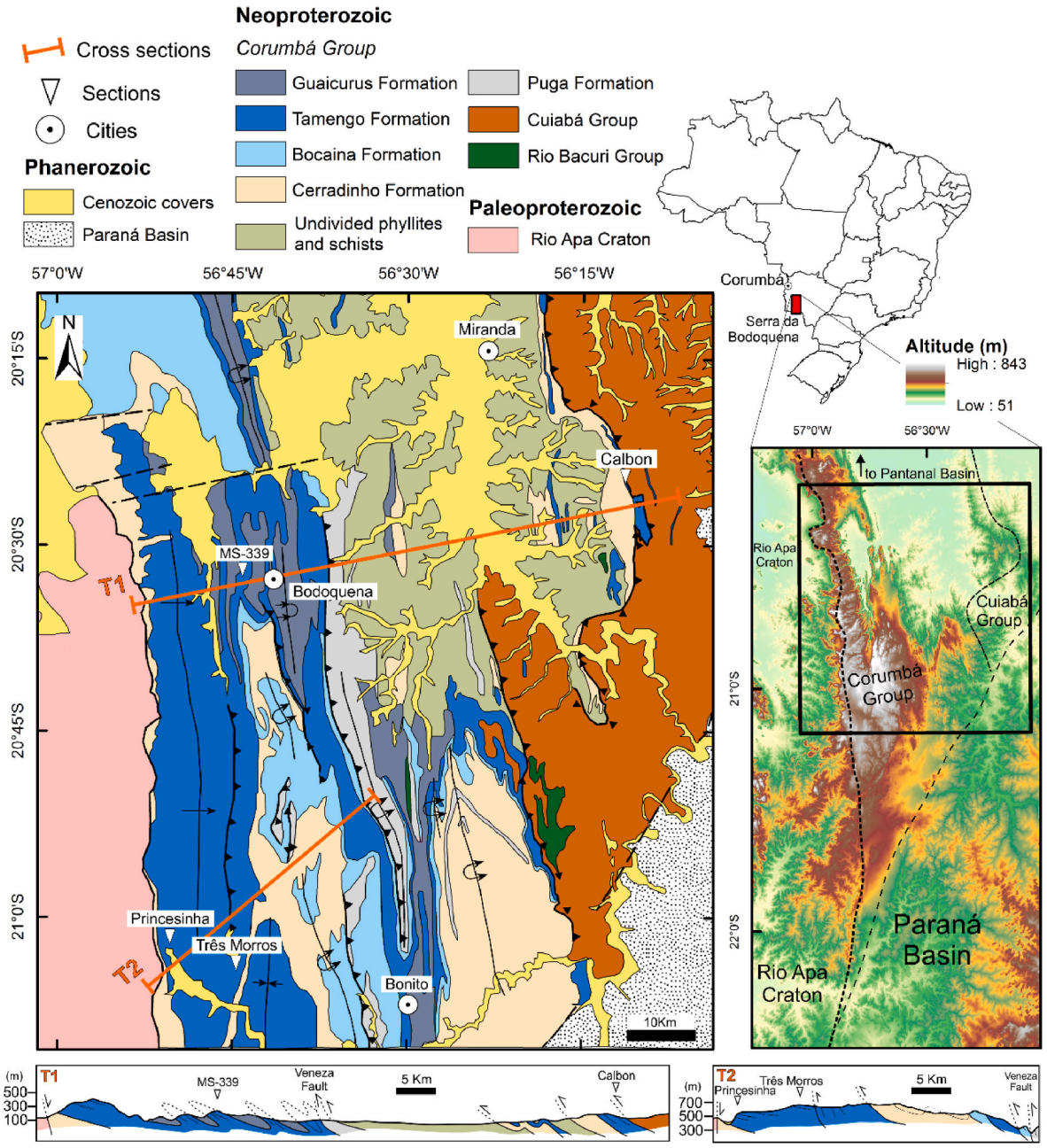

Fig. 2. Geological map of the studied area along with geological cross sections T1 and T2 (after Campanha et al., 2011) and hypsometric map of the Bodoquena Ridge. The black rectangle in the hypsometric map denotes the area of the geological map.

Glaciation, together with the Puga Formation and the upper Jacadigo Group. Intriguingly, no glacial features were documented in outcrop exposures of the Cadiueus and Cerradinho formations.

The Bocaina Formation unconformably overlies the Puga and Cerradinho formations after a major erosive surface that represents a first-order limit in the Corumbá Basin (Hippertt et al., 2023), marking the onset of widespread carbonate sedimentation. The Bocaina Formation comprises stromatolitic dolostones, often silicified, with phosphorites and shales at the top (Boggiani, 1998; Boggiani et al., 2010; Hippertt et al., 2023; Morais et al., 2021), representing a rimmed carbonate shelf, possibly restricted to the shallowest areas of the Corumbá Basin, since the Tamengo Formation directly overlies the Cerradinho Formation at many localities (Gaucher et al., 2003; Hippertt et al., 2023). The Tamengo Formation sharply overlies the Bocaina and Cerradinho formations, as well as the crystalline basement, in a major discontinuity in the Corumbá Group (Morais et al., 2021). At some localities, the contact between the Tamengo and Bocaina formations is marked by layers of polymictic breccias representing slope deposits that reworked underlying units (Fernandes et al., 2022). The Tamengo Formation hosts dark limestones interbedded with shales and siltstones, representing an extensive storm-dominated carbonate ramp (Amorim et al., 2020; Oliveira et al., 2019). Ash beds yielded U–Pb zircon ages of 555.18 ± 0.30 Ma at the top of the Bocaina Formation and of 541.85 ± 0.75 Ma at the top of the Tamengo Formation, constraining the deposition of the Tamengo Formation within this interval (Parry et al., 2017). Shales and siltstones of the Guaicurus Formation set the sedimentation of the final stages of the Corumbá Group in a last transgressive tract (Boggiani et al., 2010; Fazio et al., 2019; Walde et al., 2015).

3. Methods

3.1. Assessing sedimentological data

Four sections of the Tamengo Formation were studied in the Serra da Bodoquena region (Fig. 2). The Princesinha section is located at the westernmost part of the Corumbá Group, specifically at the Baía das Garças surroundings, where the Tamengo Formations directly overlies the Cerradinho Formation. It is composed of outcrops along the MS-382 road and on a hill, at the Princesinha Farm (21°02′29″ S, 56°51′07″ W). The Três Morros section (21°03′53″ S, 56°44′29″ W) is located 12 km east of the Princesinha section, cropping out continuously for ca. 50 m on a hill. In both Princesinha and Três Morros sections, the beds are subhorizontal. The MS-339 section (20°32′34″ S, 56°44′29″ W) is a new section exposed through recent widening of the MS-339 road, connecting Bodoquena to Morraria do Sul. In this section, the bedding strikes N20E and dips 20° to SE. The Calbon section (20°24′52″ S, 56°11′33″ W) is located at the Calbon mine, on the eastern border of the Corumbá Group. The bedding strikes N140E and dips 30° to NE. Descriptions of sedimentary facies were carried out during field work. Further sedimentological data was obtained through the description of thin sections with a Carl Zeiss Axioplan 2 petrographic microscope coupled with Leica Application Suite. Some thin sections were half-stained with alizarin red and potassium ferrocyanide following the procedure of Dias-Brito (2017) modified from Dickson (1966) to allow for the distinction between calcite and dolomite.

3.2. Major and some trace elements

Major and some trace elements were determined by X-ray fluorescence (XRF), using both glass and pressed powder pellets in the XRF Laboratory of the Institute of Geosciences of the University of São Paulo (NAP GeoAnalítica – USP). For the glass pellets, the samples were fused with lithium tetraborate ($Li_2B_4O_7$). For the powder pellets, the samples were powdered using an agate pestle down to 200 mesh and mixed with binder in a 1:5 binder to sample proportion. Pellets were analyzed on a PANanalytical AXIOS MAX Advanced X-ray Fluorescence Spectrometer. The standards used were JB-1A and JG-1A.

2.3. Rare earth elements and yttrium (REY)

The evaluation of REY of the carbonate fraction in carbonate rocks is hampered, since small amounts of detrital contamination as low as 1 % may significantly alter the obtained REY signal (Zhao et al., 2021). Therefore, different leaching methods are suggested in the literature (e.g., Tostevin et al., 2016a; Zhang et al., 2015) to digest only the carbonate fraction and eliminate detrital contaminants. The method applied here followed the procedure of Paula-Santos et al. (2020), with minor adjustments. This method aims the leaching of 15–20 % and 30–35 % of the initial mass through a two-step digestion procedure. Approximately 500 mg of sample powder was digested in 5 mL of 0.1 mol/L HCl for 60 min. Then, the solution was centrifuged, the supernatant was discarded, and the residue was rinsed with ultrapure water and centrifuged again. 20 mL of 0.1 mol/L HCl was added to the solution, which was centrifuged after 60 min of reaction. The supernatant was recovered, and the residue was rinsed with ultrapure water and centrifuged. The last supernatant was added to the retrieved solution. The leachate was dried on a hot plate and diluted in 1.25 mL of 65 % HNO_3. Finally, after one more drying step, 1.5 mL of 65 % HNO_3 was added to the residue and the solution was diluted to 50 mL with ultrapure water. The determination of trace elements, including rare earth elements and yttrium, was obtained on an iCAP Q – Thermo Scientific Inductively Coupled Plasma Mass Spectrometer (ICP-MS) in the Geochemistry Laboratory of the Institute of Geosciences, University of São Paulo. The NIST-SRM-1c reference material was prepared using the same method as the samples. One NIST-SRM-1c sample was measured after every five samples, and an average relative standard deviation of 13 % was obtained for the standard results. Additionally, three samples were measured in duplicate, yielding average relative differences of 9 % considering all elements.

Values were normalized to the Post-Archean average Australian Shale (PAAS; Pourmand et al., 2012). The $(Nd/Yb)_n$, $(Dy/Sm)_n$, and $(Tb/Yb)_n$ ratios denote the light/heavy REE (LREE/HREE), middle/light REE (MREE/LREE), and middle/heavy REE (MREE/HREE) ratios, respectively. The calculation of anomalies was carried out following the geometric average equations of Lawrence et al. (2006), where REY concentrations are normalized to PAAS:

$$(Ce/Ce^*)_n = \frac{Ce_n \times Nd_n}{Pr_n^2}$$

$$(Eu/Eu^*)_n = \frac{Eu_n}{\sqrt[3]{Sm_n^2 \times Tb_n}}$$

$$(La/La^*)_n = \frac{La_n}{Pr_n \times \left(\frac{Pr_n}{Nd_n}\right)^2}$$

3.4. Carbon and oxygen isotopes

Data for carbon and oxygen isotopes were obtained for all sections studied with exception of the Calbon section, whose isotope data were compiled from Boggiani et al. (2010). Approximately 10 mg of carbonate samples were drilled, avoiding post-depositional components such as calcite veins. The powders were then attacked by phosphoric acid and the released CO_2 was analyzed in a Thermo Fisher Scientific Delta V Advantage ICP-MS in the Laboratory of Stable Isotopes of the University of São Paulo. Results are reported using the delta notation, where:

$$\delta^{13}C_{carb} = [(^{12}C/^{13}C)_{sample} / (^{12}C/^{13}C)_{VPDB} - 1] \times 1000$$

And

$$\delta^{18}O_{carb} = [(^{16}O/^{18}O)_{sample} / (^{16}O/^{18}O)_{VPDB} - 1] \times 1000$$

The isotopic ratios were normalized as per the Vienna Pee-Dee Belemnites (VPDB) reference material and expressed in parts per mille (‰). The average long-term reproducibility was ±0.10 ‰ for $\delta^{13}C_{carb}$ and ±0.09 ‰ for $\delta^{18}O_{carb}$.

4. Results

4.1. Sedimentology and stratigraphy

The Princesinha section directly overlies a 15 m thick succession of arkosic sandstone of the Cerradinho Formation, thus representing the basal Tamengo Formation in the Serra da Bodoquena region. The lower section is mainly composed of ooid grainstones with swaley and hummocky cross-bedding interbedded with shales (Fig. 3). There are also thin (ca. 30 cm) intercalations of carbonate intraformational breccias and poorly sorted coarse sandstones. In the surroundings of the Princesinha Section, there are carbonate facies with microbial lamination and thrombolite occurrences associated with grainstones approximately in the same stratigraphic level of the lower section (Fig. 3). The upper Princesinha section is mainly composed of oolitic grainstones with swaley and wavy cross-bedding, mudstones, and rare shale intercalations. Pyrite framboids are present throughout the entire Princesinha section, with an average diameter of 6.8 μm. Euhedral pyrite crystals up to 50 μm were observed only in the lower carbonate beds. The stained thin sections reveal that the samples from the upper section are partially and locally dolomitized.

The Três Morros section displays dark mudstones passing to ooid

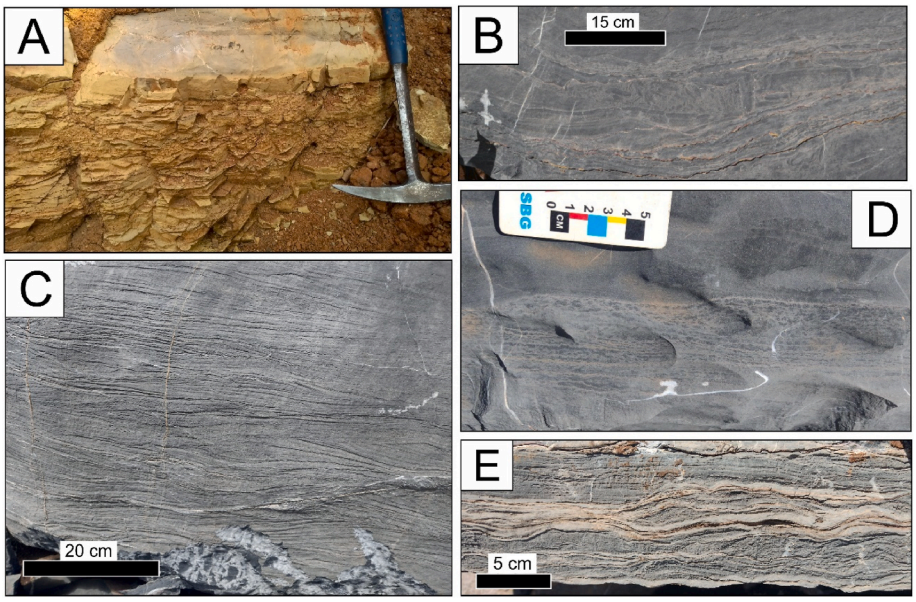

Fig. 3. Facies of the Tamengo Formation in the Princesinha section and its surroundings. (A) Contact between limestone (top) and siltstone (bottom) in the lower Princesinha section. (B) Carbonate intraformational breccia. (C) Grainstone with swaley cross-bedding. (D) Thrombolite. (E) Microbial lamination.

grainstones in metre-scale coarsening-upward successions. These rocks exhibit wavy sub-horizontal undulating bedding (Fig. 4). The oolitic grainstones show highly micritized ooids around 150 μm in diameter (Fig. 5). In this section, pyrite framboids are ubiquitous, with an average framboid diameter of 5.7 μm. Some thin sections also presented euhedral pyrites. The stained thin sections show a low degree of dolomitization, with minor dolomitized portions (Fig. 4).

The MS-339 section is highly deformed, presenting intrafoliation folds, which can cause an overestimation of the original thickness of the succession. In its lower and middle parts, it displays intercalations of marly limestones with shale lens and shales with carbonate lens (Fig. 4). In these sectors, there are rare intercalations of fine silty sandstone with carbonate lens. The upper MS-339 section is dominated by a thick limestone succession, locally with brecciated fabric (Fig. 5), interbedded with marls with shale lens. Due to the high degree of deformation and micritization of this section, it was not possible to determine the nature of the carbonate facies, as many of the original constituents were obliterated. All three sectors of the MS-339 section show pyrite framboids, with an average diameter of 7.9 μm. The degree of dolomitization is relatively high in the mid-section, achieving around 50 % of the carbonate mass (Fig. 5).

4.2. *Isotope chemostratigraphy*

In the Princesinha section, the lower 32 m presented $\delta^{13}C_{carb}$ values ranging from −1.33 ‰ to +2.00 ‰, while the upper section yielded values spanning from +2.26 to 5.52 ‰ (Fig. 6). The oxygen isotopes in this section ranged from −7.53 to −3.97 ‰, with higher variation in the

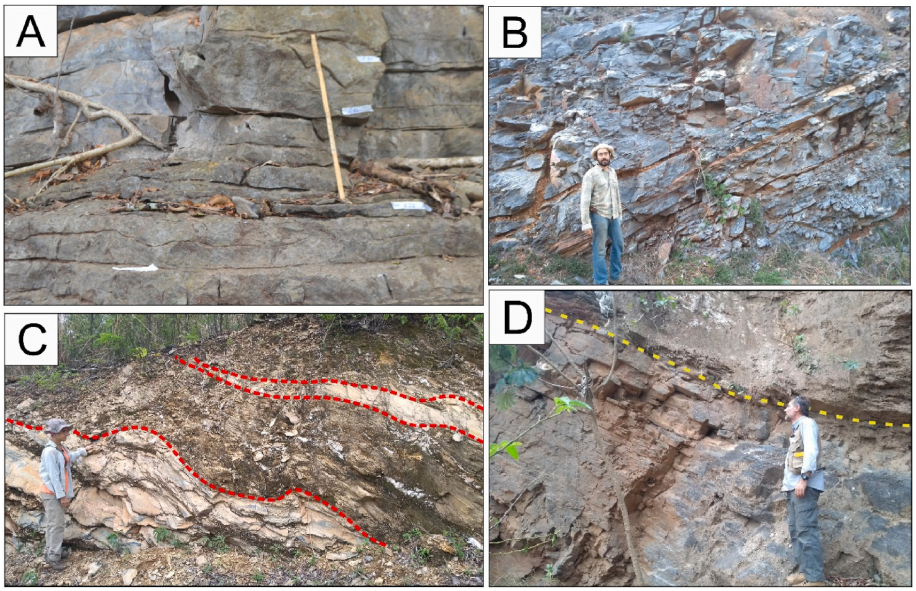

Fig. 4. (A) Oolitic grainstone sequence in the Três Morros section with undulating bedding. Scale is 40 cm long. (B) Grainstone-dominated sequence in the upper MS-339 section. (C) Marl and shale intercalations (red dashed lines represent contacts) in the middle MS-339 section. (D) Contact (yellow dashed line) between dolarenite (bottom) and phyllite (top) in the upper Calbon section.

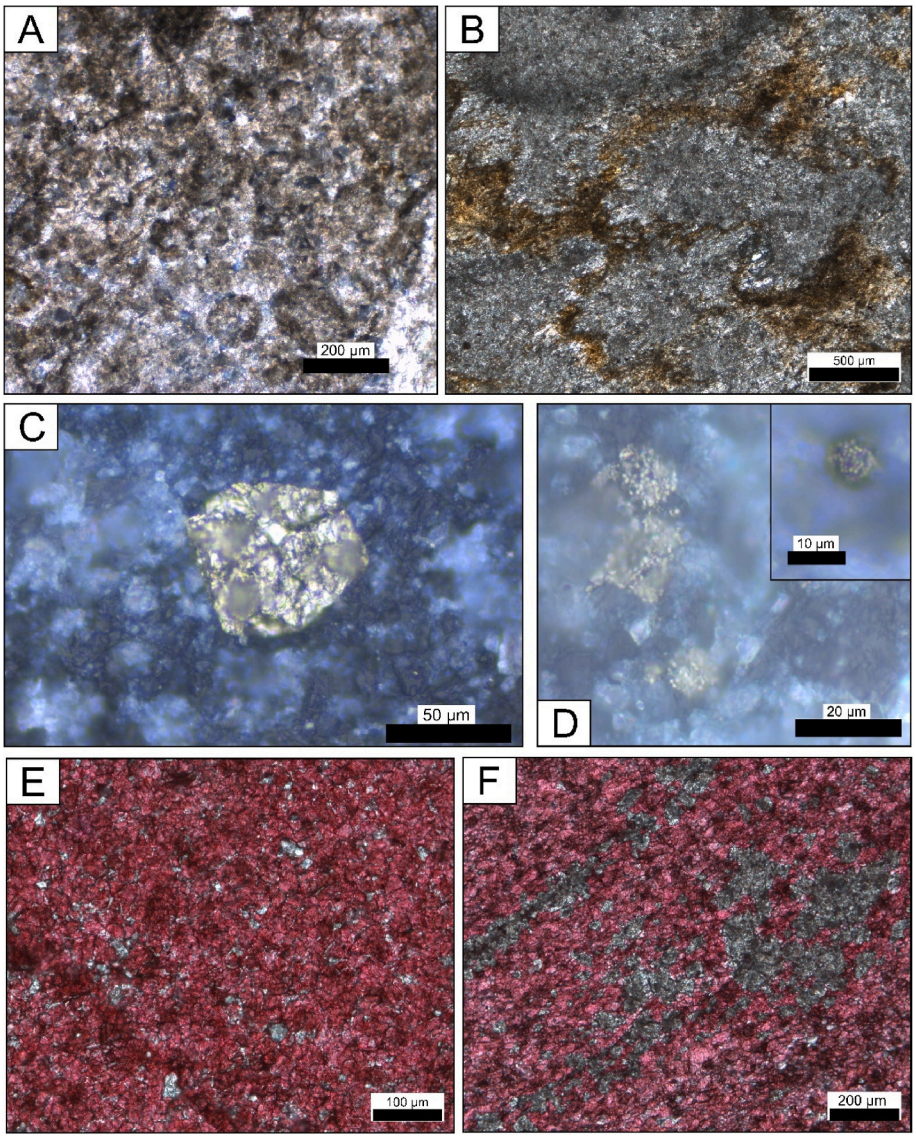

Fig. 5. (A) Ooid grainstone facies in the Três Morros section with micritized ooids. (B) Brecciated fabric in the middle MS-339 section. (C) Euhedral pyrite in the Princesinha section. (D) Pyrite framboid in cluster and isolated, in the MS-339 section. (E) Photomicrograph of stained thin section (pink color indicates calcite) of the Três Morros section, showing predominance of calcite. (F) Stained thin section of the MS-339 section, showing a medium degree of dolomitization.

lower section. The Três Morros section displayed relatively high shifts in $\delta^{13}C_{carb}$, from +1.65 to +4.25 ‰ and $\delta^{18}O_{carb}$ spanning from −6.24 to −4.03 ‰, in a considerably stable trend. The $\delta^{13}C_{carb}$ curve in the MS-339 section showed stable values in the lower and middle part, around +3 and + 2 ‰, respectively. In the upper section, the $\delta^{13}C_{carb}$ curve shows a decreasing trend, from 2.94 to 1.10 ‰, with two minor negative excursions down to −1.19 ‰. Oxygen isotopes are relatively stable around −5 ‰, with exception of the middle section, which exhibited considerably lighter oxygen isotope composition, around −12 ‰ (Fig. 6). Complete data is given in Table 1.

4.3. Rare earth elements and yttrium (REY)

Samples from the Princesinha section displayed ∑REY ranging from 0.90 to 11.93 ppm, an average positive $(La/La^*)_n$ of 0.84, absent to slightly positive Ce anomalies up to 1.15, and Y/Ho ranging from 49 to 77 (Fig. 7). The REY distribution of the Três Morros samples showed lower ∑REY, of around 0.20 ppm, absent to slightly negative Ce anomalies down to 0.92, absent La anomalies (average $(La/La^*)_n$ of 0.97), and high Y/Ho ratios up to 74. Notable MREE-bulge pattern is observed in both Princesinha and Três Morros sections, verified through $(Tb/Yb)_n$ ratios, which yielded an average of 1.48, and $(Dy/Sm)_n$, whose average was 0.93, considering both sections. Also, the same samples presented average $(Nd/Yb)_n$ of 1.28, indicating general HREE depletion.

Samples from the Calbon section yielded variable ∑REY, from 0.20 to 6.10 ppm, slightly negative Ce anomalies down to 0.90, Y/Ho of 36 and 44 and La anomalies from 1.21 to 1.99. Two samples from the Calbon section also presented low $(Nd/Yb)_n$ ratios (0.54 and 0.85), showing a HREE enrichment (Fig. 7), in contrast with the other sections. One sample from the MS-339 section yielded a prominent $(Eu/Eu^*)_n$ of 4.20. The Eu for the other sample was below detection limit. Both samples from the MS-339 section presented positive $(La/La^*)_n$ of 1.24 and 1.50, and $(Ce/Ce^*)_n$ of 1.05 and 0.95. All values are displayed in Table 2.

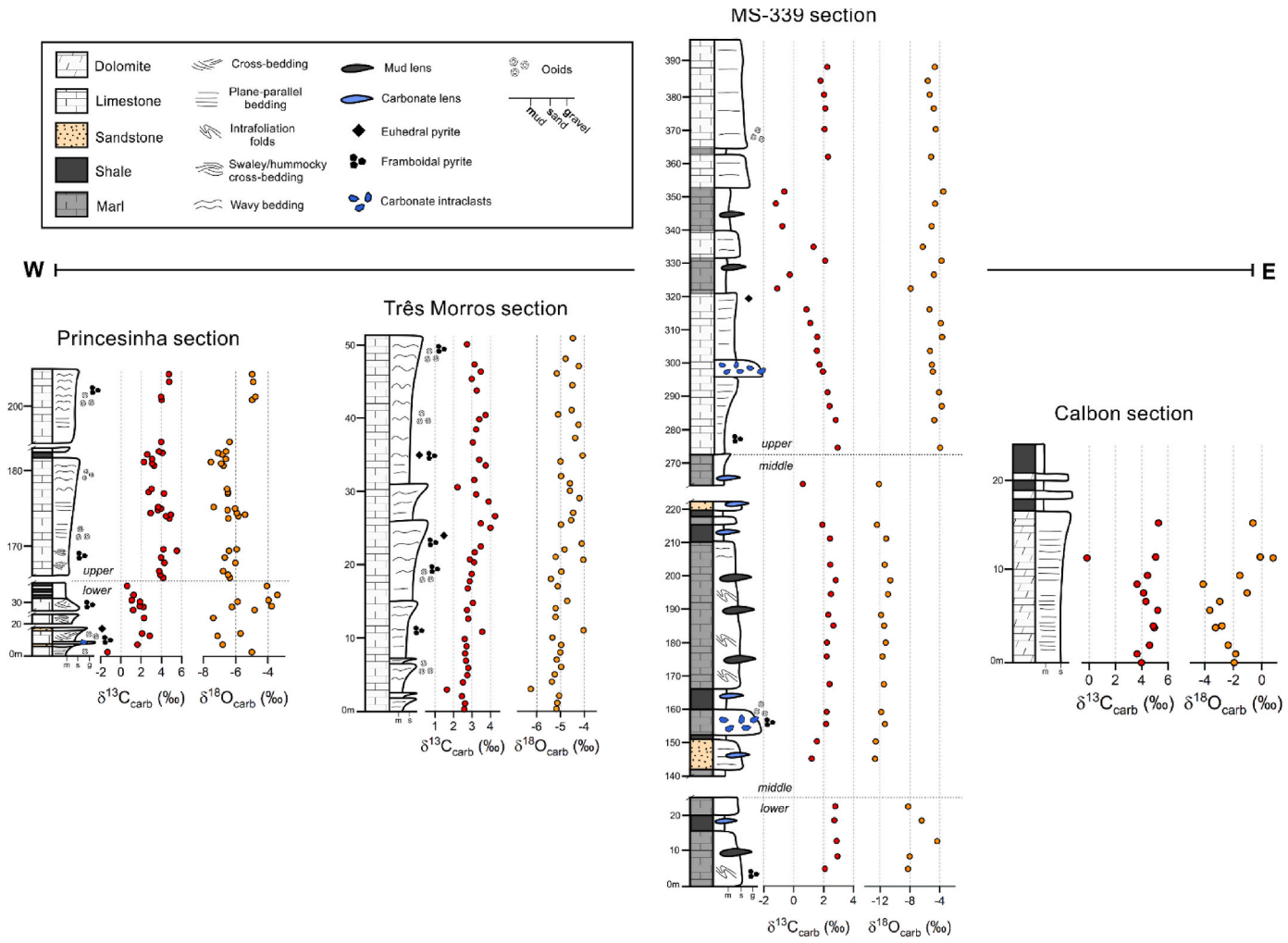

Fig. 6. Sedimentological and C and O isotope data of the studied sections. Isotope data from the Calbon section is from Boggiani et al. (2010).

5. Discussion

5.1. Depositional setting of the Tamengo Formation at the Serra da Bodoquena region

The layers of shales and siltstones, abundant in the lower Princesinha and MS-339 sections, suggest low energy bottom conditions, with sedimentation of fine particles by suspension fallout (Reading, 1996). In the same sections, ooid grainstones with hummocky and swaley cross-bedding indicate deposition below fair-weather wave base level and above storm wave base level, allowing for the preservation of such structures after storm cease (Dott and Bourgeois, 1982). In that context, fine sedimentation occurred between major storms (Amorim et al., 2020; Labaj and Pratt, 2016). The monotonous oolitic grainstone successions of the upper Princesinha and Três Morros sections indicate a high energy setting. Such facies are traditionally associated with shallow water carbonate systems (Burchette and Wright, 1992). The presence of hummocky, swaley, and wavy structures in these rocks also indicates reworking by storm waves and possibly fair-weather waves (Tucker and Wright, 1990) at relatively shallow depths (Dumas and Arnott, 2006). The thin beds of intraclastic carbonate breccias in the lower Princesinha and MS-339 sections indicate reworking of lithified carbonate beds in a moderate to high energy setting.

The two defining criteria of Amorim et al. (2020) to interpret a storm-dominated carbonate ramp from the type sections of the Tamengo Formation in Corumbá are also found in the Serra da Bodoquena region. Firstly, a carbonate ramp implies a lateral continuity of facies, which is verified in the sections studied herein and by Boggiani et al. (2010), achieving an even greater lateral continuity (ca. 60 km) compared to the Corumbá region (ca. 7 km). Secondly, the greatest difference between a carbonate ramp and a carbonate rimmed platform is the sedimentary facies associated with extensive build-ups that constitutes the rim. The Tamengo Formations lacks that type of facies, with only minor microbialites in association with oolitic grainstones in inner and mid-ramp settings (Oliveira et al., 2019). Minor occurrences of stromatolites and thrombolites may fairly be present in mid to outer ramp settings, composing isolated build-ups rather than a barrier, such as in the case of rimmed shelves (Burchette and Wright, 1992). Hence, it is safe to assume that the extension of the Tamengo Formation carbonate ramp (Amorim et al., 2020; Oliveira et al., 2019; Ramos et al., 2022) exceed the well-known region of Corumbá, encompassing the Tamengo Formation exposures in the Serra da Bodoquena region as well. In this scenario, the Princesinha, Três Morros, and MS-339 sections are consistent with a mid to outer ramp setting, since they show varying degrees of storm influence, with hummocky and swaley cross-bedding (Burchette and Wright, 1992). Furthermore, mid to outer ramp sectors also have large amounts of lime and/or terrigenous mud, precipitated from fallout during low-energy intervals, in agreement with the marly facies in the MS-339 section and the shale intercalations in the Princesinha and MS-339 sections.

The Calbon section, on the other hand, represents a deep-water setting, with high terrigenous input, represented by the abundant

Table 1
Carbon and oxygen isotope data, Sr concentration, Mn/Sr, and Mg/Ca ratios of the samples from the Tamengo Formation.

	Sample	ICP-MS		XRF		
		$\delta^{13}C_{carb}$‰ (VPDB)	$\delta^{18}O_{carb}$‰ (VPDB)	Sr (ppm)	Mn/Sr (ppm/ppm)	Mg/Ca (%/%)
Princesinha section	BG - 0,6	−1.33	−5.00	324	1.0996	0.4271
	BG - 1,5	1.63	−6.80			
	BG - 16,8	2.84	−7.12	449	0.1035	0.0497
	BG - 17,2	2.08	−5.70			
	BG - 22,9	2.28	−7.38	484	0.2560	0.0407
	BG - 26,6	1.21	−4.83			
	BG - 27,1	2.21	−6.23			
	BG - 27,2	1.86	−3.78			
	BG - 27,8	1.88	−5.88			
	BG - 28,0	1.06	−3.97	398	0.6616	0.3008
	BG - 28,8	1.25	−3.43			
	BG - 29,8	0.61	−4.07			
	BG - 40,6	4.16	−6.36	2475	0.0688	0.0217
	BG - 40,8	4.09	−6.4			
	BG - 41,0	3.88	−6.46			
	BG - 41,5	3.78	−6.77			
	BG - 42,6	4.30	−6.01			
	BG - 43,0	1.37	−5.30			
	BG - 43,3	3.95	−6.67			
	BG - 44,2	5.52	−6.41			
	BG - 44,4	4.19	−5.94	4324	0.0125	0.0103
	BG - 48,5	4.80	−6.45			
	BG - 48,8	4.46	−5.84			
	BG - 49,0	4.92	−5.43			
	BG - 49,2	2.93	−5.93			
	BG - 49,6	3.66	−6.5	3701	0.0230	0.0146
	BG - 49,8	3.95	−6.03			
	BG - 50,0	3.68	−7.36			
	BG - 51,6	4.21	−5.47			
	BG - 51,8	4.25	−6.48			
	BG - 52,0	2.73	−6.48			
	BG - 52,4	3.03	−6.53			
	BG - 55,5	3.27	−6.75	3885	0.1435	0.0144
	BG - 55,8	3.09	−6.9			
	BG - 56,0	2.26	−7.53			
	BG - 56,2	3.08	−6.61			
	BG - 57,0	2.59	−6.83			
	BG - 57,2	4.09	−7.08			
	BG - 57,4	3.76	−6.6			
	BG - 70,0	3.97	−6.37	4626	0.0301	0.0132
	BG - 75,5	4.01	−4.98	4405	0.0211	0.0082
	BG - 76,0	3.95	−4.78			
	BG - 78,0	4.76	−4.92			
	BG - 79,0	4.73	−4.98	4214	0.0165	0.0077
Três Morros section	3 M - 0,3	2.58	−5.16	3922	0.0039	0.0040
	3 M - 1,1	2.62	−5.13			
	3 M - 2,1	2.45	−5.05			
	3 M - 3,0	1.65	−6.24			
	3 M - 4,0	2.51	−5.36			
	3 M - 5,0	2.75	−5.24	3289	0.0071	0.0037
	3 M - 6,0	2.80	−4.97			
	3 M - 7,0	2.68	−5.15			
	3 M - 8,0	2.63	−5.00			
	3 M - 9,0	2.71	−4.97			
	3 M - 10,0	2.61	−5.34	3860	0.0040	0.0037
	3 M - 11,0	3.56	−4.03			
	3 M - 12,8	2.80	−5.20			
	3 M - 14,0	2.73	−5.20			
	3 M - 15,0	3.06	−4.71	4236	0.0037	0.0031
	3 M - 17,0	2.78	−5.11			
	3 M - 18,0	2.88	−5.40			
	3 M - 19,0	2.98	−4.96			
	3 M - 20,6	3.12	−4.04	3873	0.0080	0.0056
	3 M - 21,0	2.89	−5.20			
	3 M - 22,0	3.15	−4.82			
	3 M - 22,8	3.48	−4.11			
	3 M - 25,4	4.01	−4.98	4284	0.0054	0.0043
	3 M - 26,0	3.48	−4.55			
	3 M - 27,0	4.25	−4.46			
	3 M - 29,0	3.91	−4.20			
	3 M - 30,0	3.23	−4.60	3842	0.0040	0.0037
	3 M - 31,0	2.21	−4.97			
	3 M - 32,0	3.13	−5.00			

(*continued on next page*)

Table 1 (*continued*)

	Sample	ICP-MS		XRF		
		$\delta^{13}C_{carb}$‰ (VPDB)	$\delta^{18}O_{carb}$‰ (VPDB)	Sr (ppm)	Mn/Sr (ppm/ppm)	Mg/Ca (%/%)
	3 M - 34,0	3.75	−4.07			
	3 M - 34,8	3.41	−4.38			
	3 M - 37,2	3.05	−4.24			
	3 M - 39,0	3.23	−5.10			
	3 M - 40,4	3.40	−4.58			
	3 M - 41,0	3.74	−4.53			
	3 M - 44,4	3.26	−4.49	3408	0.0091	0.0048
	3 M - 46,0	2.99	−5.15			
	3 M - 47,0	3.48	−4.23			
	3 M - 48,0	3.14	−4.79			
	3 M - 50,8	2.73	−4.48	3970	0.0059	0.0056
MS-339 section	22 BD 21–0,7	2.95	−8.03	3697	0.0251	0.0038
	22 BD 21 - 5	2.09	−8.24			
	22 BD 21–8,7	2.93	−8.02			
	22 BD 21 - 13	2.87	−4.34			
	22 BD 21 - 19	2.72	−6.43			
	22 BD 21 - 23	2.78	−8.22			
	23 BD 21 - 6	1.20	−12.65			
	23 BD 21 - 12	1.55	−12.56			
	23 BD 21 - 16	2.17	−11.33			
	23 BD 21 - 20	2.20	−11.83			
	23 BD 21 - 28	2.40	−11.47			
	23 BD 21 - 36	2.20	−11.67			
	23 BD 21 - 40	2.22	−11.23			
	23 BD 21–44,35	2.65	−11.43			
	23 BD 21 - 48	2.31	−11.86			
	23 BD 21 - 54	2.49	−10.93			
	23 BD 21 - 58	2.81	−10.61			
	23 BD 21 - 62	2.45	−11.35			
	23 BD 21 - 70	2.43	−11.17			
	23 BD 21 - 74	1.92	−12.40			
	24 BD 21 - 2	0.61	−12.12			
	24 BD 21 - 8	2.31	−6.21	2862	0.0216	0.0056
	24 BD 21 - 12	2.94	−3.95			
	24 BD 21 - 20	2.81	−4.73			
	24 BD 21 - 24	2.40	−3.74			
	24 BD 21 - 28	2.26	−4.10			
	24 BD 21 - 34	1.95	−4.93			
	24 BD 21 - 36	1.72	−5.05			
	24 BD 21 - 40	1.55	−5.31			
	24 BD 21 - 44	1.57	−3.70			
	24 BD 21 - 48	1.10	−3.88			
	24 BD 21 - 52	0.86	−5.39			
	24 BD 21 - 58	−1.09	−7.89			
	24 BD 21 - 62	−0.26	−4.79			
	24 BD 21 - 66	2.10	−3.78			
	24 BD 21 - 70	1.32	−6.29			
	24 BD 21 - 72	0.88	−5.69	1905	0.0041	0.0105
	24 BD 21 - 76	−0.76	−5.09			
	24 BD 21–82,5	−1.19	−4.63			
	24 BD 21 - 86	−0.63	−3.52			
	24 BD 21 - 96	2.29	−5.16			
	24 BD 21 - 104	2.06	−4.56			
	24 BD 21 - 110	2.11	−4.80			
	24 BD 21 - 114	2.03	−5.37			
	24 BD 21 - 118	1.79	−5.61			
	24 BD 21 - 122	2.24	−4.67			
	24 BD 21 - 128	2.57	−5.02	3453	0.0045	0.0038

quartz grains in the dolomites (Boggiani et al., 2010). In this case, the sedimentation of the dolarenite facies occurred through high-energy mass movements, followed by periods of low-energy, in which fine sedimentation dominated.

Euhedral and framboidal pyrites are ubiquitous in the Princesinha, Três Morros and MS-339 sections. Euhedral pyrites are indicative of saturation of Fe monosulfides in anoxic diagenetic environments (Wang et al., 2012; Wilkin et al., 1996). Framboids may be syngenetic, i.e., precipitated from euxinic water column, or diagenetic, formed in pore waters with overlying oxic/dysoxic water column (Blood et al., 2020; Wang et al., 2013). The mean diameters of the pyrite framboids of the studied sections suggest a mixture of syngenetic and diagenetic pyrites under water column shifting ephemerally from dysoxic to sulfidic (Wang et al., 2012).

5.2. Evaluation of the isotope geochemical signal

Some major and trace elements such as Fe, Mn, and Sr, are sensitive to diagenetic alterations and may be used to track the extent of isotope diagenetic alteration (Banner and Hanson, 1990; Ullmann and Korte, 2015). As Sr tends to leave the carbonate mineral lattice during fluid-rock interaction and non-marine calcites are relatively Mn-rich, Sr concentrations and elemental ratios, such as Mn/Sr, are good indicators of diagenetic overprint (Banner and Hanson, 1990; Kim et al., 2012).

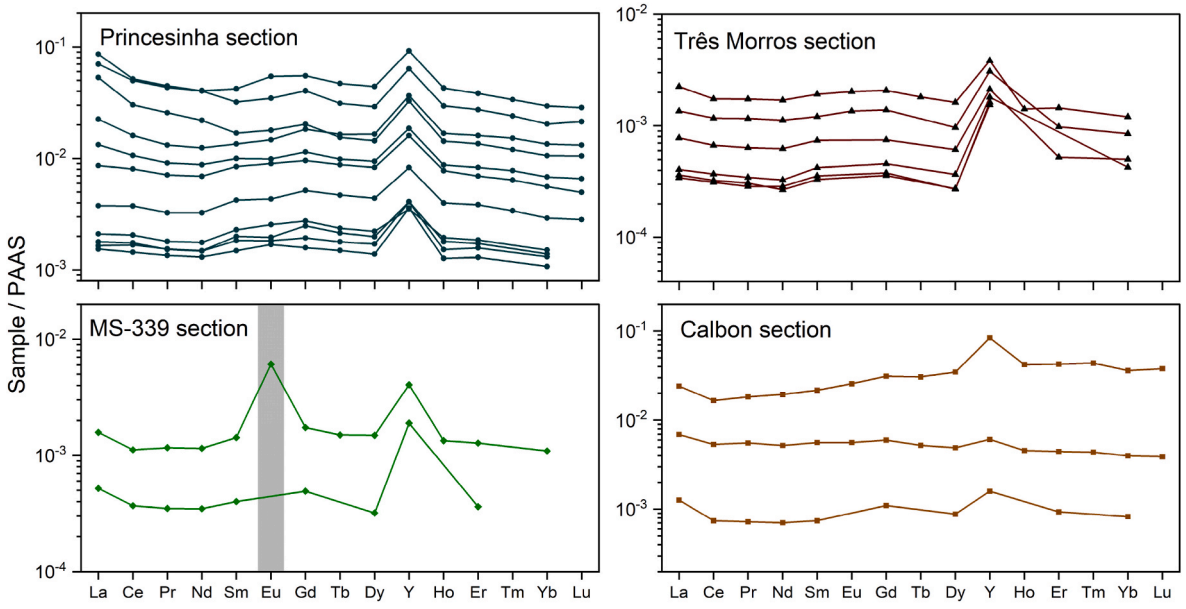

Fig. 7. PAAS-normalized REY patterns of samples from the studied sections. Data is displayed in Table 2.

Originally, carbonates with Mn/Sr > 2 are assigned as altered (Brand and Veizer, 1980; Veizer, 1983), but Kaufman and Knoll (1995) extended this threshold level to 10. However, specific cut-off values are not recommended, and each dataset should be carefully evaluated. The samples analyzed in this work show Mn/Sr ratios up to 1.1, which implies an overall negligible diagenetic overprint. However, there is a clear trend between Mn/Sr and $\delta^{13}C_{carb}$, with samples from the lower Princesinha section presenting the most altered signals (Fig. 8), suggesting some degree of diagenetic influence on the carbon isotope record of these samples. The cut-off value of 0.4 Mn/Sr was used to determine the threshold of unaltered samples. The two samples above 0.4 Mn/Sr were discarded from the paleoenvironmental interpretations. The same samples showed higher Mg/Ca ratios, up to 0.43 (Fig. 8), indicating a higher degree of dolomitization, also verified through stained thin sections.

In the Três Morros and middle MS-339 sections, there is a significant positive covariation ($R^2 = 0.54$ and $R^2 = 0.78$, respectively) between $\delta^{13}C_{carb}$ and $\delta^{18}O_{carb}$ (Fig. 9). This covariation is traditionally associated with diagenetic alteration by meteoric fluids (Allan and Matthews, 1982), but can also be the result of marine-freshwater mixing conditions (Swart and Oehlert, 2018). The other sections do not show significant covariations between these parameters. Importantly, also in the middle MS-339 section, there is a significant drop in the $\delta^{18}O_{carb}$ record down to −12 ‰, which may be related to the percolation of high-T fluids. This scenario will be discussed in the REY section.

5.3. Isotope chemostratigraphy of the Tamengo Formation in the Serra da Bodoquena region

The carbon isotope record of the Tamengo Formation in the Serra da Bodoquena region is marked by positive $\delta^{13}C_{carb}$, with few, short-lived excursions towards lower values, but often not reaching negative values. The $\delta^{13}C_{carb}$ curves of the studied sections are in general good agreement with the sections studied by Boggiani et al. (2010) at the same region. Furthermore, the general positive values of $\delta^{13}C_{carb}$ contrast with the other carbonate successions at Serra da Bodoquena region. For instance, the Puga cap dolostone displays negative values around −5 ‰ (Boggiani et al., 2003; Spangenberg et al., 2014), typical of post-Marinoan cap carbonates, and the dolomites of the Bocaina Formation exhibit $\delta^{13}C_{carb}$ around 0 ‰ (Alvarenga et al., 2011; Boggiani, 1998). Therefore, the positive $\delta^{13}C_{carb}$ plateau recorded in all studied sections appears to be restricted to the Tamengo Formation in the area.

Considering the sections investigated here and by Boggiani et al. (2010), the Tamengo Formation shows decreasing average $\delta^{13}C_{carb}$ values from west to east, with exception of the Calbon section, which yielded the highest $\delta^{13}C_{carb}$ signature. Furthermore, in the upper MS-339 section, the two short-lived negative $\delta^{13}C_{carb}$ excursions are linked to facies variations, as their occur in marly facies interbedded with shales, while the grainstones present higher $\delta^{13}C_{carb}$ values. Similarly, in the Princesinha section, the carbonate beds in the lower section show lower $\delta^{13}C_{carb}$ values, while the monotonous grainstones of the upper section display higher $\delta^{13}C_{carb}$. Such regional and local variations on the $\delta^{13}C_{carb}$ record may be linked to an isotope depth gradient caused by seawater redox stratification (Giddings and Wallace, 2009). In fact, there are strong evidence that support a Late Neoproterozoic stratified ocean, with a thin layer of oxic surface waters overlying ferruginous (i.e., Fe(II)-enriched) bottom waters, and sulfidic (euxinic) water wedges impinging in the continental shelves (Canfield et al., 2008; Frei et al., 2013, 2017; Li et al., 2010), in several Ediacaran basins, including the Tamengo Formation in Corumbá (Spangenberg et al., 2014). In such scenario, bottom waters would host a large dissolved organic carbon (DOC) pool, which, after remineralization during sulfate reduction processes, would result in a ^{13}C-depleted dissolved inorganic carbon (DIC) reservoir in bottom waters, ultimately developing a large carbon isotope depth gradient (Jiang et al., 2007).

There is also an increasing trend in the average $\delta^{18}O_{carb}$ from west to east considering all sections in the Serra da Bodoquena region. The Princesinha section, in the westernmost part of the Corumbá Group, for instance, presented average $\delta^{18}O_{carb}$ of −5.9 ‰, while the Calbon section, at the eastern limit of the Corumbá Group, displayed average $\delta^{18}O_{carb}$ of −1.9 ‰. This trend is the opposite of what would be expected considering that the oxygen isotopes signatures were completely altered by post-depositional hydrothermal fluids, as metamorphism and deformation are more intense to the east and hydrothermal fluids have distinct lighter isotope signature compared to marine carbonates (Kaufman and Knoll, 1995). Therefore, this oxygen isotope profile must reflect original basin features. The relatively low $\delta^{18}O_{carb}$ values in the western sections may be explained by the influence of meteoric fluids (Swart and Oehlert, 2018), which has lower $\delta^{18}O_{carb}$ compared to marine carbonates and affects shallower regions. The influence of meteoric diagenesis verified in the Três Morros and MS-339 sections, as discussed

Table 2
PAAS-normalized REY data and related parameters of the samples from the Tamengo Formation.

	BG − 0,6	BG − 16,8	BG − 22,9	BG − 28,0	BG − 40,6	BG − 44,4	BG − 49,4	BG − 55,5	BG − 70,0	BG − 75,0	BG − 79,0	3M − 0,3	3M − 15,0	3M − 20,6	3M − 25,4	3M − 44,4	3M − 50,8	Calbon − 0,0	Calbon − 2,0	Cabon − 4,5	22BD21 − 0,7	23BD21 − 26
La	0.08617	0.0021	0.02241	0.05306	0.01326	0.00377	0.00165	0.07015	0.00863	0.00178	0.00153	3.43E-04	4.07E-04	0.00224	0.00135	3.63E-04	7.78E-04	0.00693	0.00127	0.02399	5.19E-04	0.00158
Ce	0.05167	0.00205	0.01601	0.03017	0.01064	0.00374	0.00167	0.04978	0.00807	0.00174	0.00144	3.12E-04	3.70E-04	0.00175	0.00117	3.25E-04	6.69E-04	0.00538	7.42E-04	0.01656	3.69E-04	0.00112
Pr	0.04468	0.00179	0.01315	0.02566	0.00912	0.00325	0.00154	0.04316	0.00712	0.00152	0.00135	2.86E-04	3.46E-04	0.00174	0.00116	3.07E-04	6.36E-04	0.00558	7.22E-04	0.0182	3.49E-04	0.00117
Nd	0.04025	0.00176	0.01241	0.02191	0.0088	0.00326	0.00148	0.04045	0.00691	0.00147	0.0013	2.86E-04	3.27E-04	0.0017	0.00112	2.67E-04	6.24E-04	0.00523	7.05E-04	0.01942	3.47E-04	0.00115
Sm	0.032	0.00228	0.01344	0.0168	0.01	0.00423	0.00199	0.04205	0.00847	0.00183	0.00148	3.57E-04	4.24E-04	0.00193	0.00121	3.31E-04	7.38E-04	0.00564	7.42E-04	0.02162	4.00E-04	0.00143
Eu	0.03467	0.00254	0.01467	0.01783	0.0099	0.00433	0.00196	0.05441	0.009	0.00182	0.00169	< LD	< LD	0.00203	0.00135	< LD	< LD	0.00564	< LD	0.0256	< LD	0.00609
Gd	0.04034	0.00274	0.01821	0.02019	0.01145	0.00516	0.00248	0.05509	0.00958	0.00193	0.00158	3.78E-04	4.59E-04	0.00208	0.00139	3.59E-04	7.48E-04	0.006	0.0011	0.03117	4.91E-04	0.00174
Tb	0.03114	0.00236	0.01637	0.01541	0.00986	0.0047	0.00214	0.04688	0.00881	0.00178	0.00149	< LD	< LD	0.00182	< LD	< LD	< LD	0.00523	< LD	0.03063	< LD	0.0015
Dy	0.02904	0.00221	0.01647	0.01437	0.00944	0.0044	0.00198	0.04408	0.00831	0.0017	0.00138	2.70E-04	3.68E-04	0.00162	9.62E-04	2.74E-04	6.12E-04	0.00493	8.81E-04	0.03461	3.19E-04	0.00149
Y	0.06372	0.00353	0.03653	0.03265	0.01857	0.0083	0.0041	0.09221	0.01597	0.00407	0.0036	0.00163	0.00181	0.00384	0.00308	0.00154	0.00213	0.00611	0.00159	0.08383	0.00189	0.00404
Ho	0.02954	0.00194	0.01674	0.01426	0.00877	0.00398	0.00179	0.04278	0.00777	0.00151	0.00127	< LD	< LD	0.00141	< LD	< LD	< LD	0.00458	< LD	0.04212	< LD	0.00134
Er	0.02733	0.00185	0.016	0.01352	0.00831	0.00384	0.00172	0.03832	0.00696	0.00157	0.00129	< LD	< LD	0.00145	9.76E-04	< LD	5.24E-04	0.00447	9.31E-04	0.04267	3.62E-04	0.00128
Tm	0.024	< LD	0.01517	0.01198	0.00779	0.0034	< LD	0.0337	0.00641	< LD	< LD	< LD	< LD	< LD	< LD	< LD	< LD	0.00437	< LD	0.04357	< LD	< LD
Yb	0.02029	0.0015	0.01343	0.01058	0.00683	0.00291	0.00138	0.02952	0.0056	0.00131	0.00107	< LD	4.25E-04	0.0012	8.49E-04	< LD	5.01E-04	0.00399	8.24E-04	0.03594	< LD	0.00109
Lu	0.02132	< LD	0.01314	0.01052	0.00659	0.00282	< LD	0.02856	0.00496	< LD	< LD	< LD	< LD	< LD	< LD	< LD	< LD	0.00392	< LD	0.03777	< LD	< LD
Eu/Eu*	1.09352	1.10219	1.02139	1.09236	0.99509	0.9896	0.9599	1.24785	1.04919	1.00757	1.13619			1.07529				1.0244		1.05418		4.19665
Ce/Ce*	1.04171	1.11871	1.14913	1.00423	1.12413	1.15171	1.0497	1.0809	1.10054	1.11054	1.03165	1.09086	1.01178	0.9826	0.96941	0.91686	1.03084	0.90296	1.00455	0.97114	1.052	0.94629
La/La*	1.01225	0.75829	0.84035	0.92787	0.85195	0.76139	0.7722	0.93087	0.78431	0.72593	0.87621	0.92127	0.85955	1.22049	1.0529	0.75456	1.00942	1.21644	1.54389	1.99297	1.24744	1.50412
Y/Ho	2.1569	1.8193	2.18234	2.29012	2.11825	2.08481	2.2906	2.15567	2.05595	2.68682	2.84116			2.71681				1.3348		1.99033		3.01286
Nd/Yb	1.98352	1.17227	0.92409	2.07142	1.28748	1.11807	1.07082	1.37036	1.23467	1.12513	1.21319		0.76931	1.41364	1.31982		1.24386	1.30951	0.85556	0.54031		1.0546
Dy/Sm	0.90766	0.9695	1.22492	0.85556	0.94402	1.04041	0.99486	1.0483	0.98104	0.93243	0.9336	0.75724	0.86974	0.84094	0.79666	0.82898	0.82935	0.87267	1.18652	1.60108	0.79929	1.04219
Tb/Yb	1.53463	1.57252	1.21951	1.45717	1.44305	1.61156	1.54635	1.58817	1.574	1.362	1.388			1.50942				1.31165		0.85222		1.37066
∑REY	11.63032		4.03068	6.65684	2.46282	0.9072		11.93668	1.89566									1.2087		6.09417		
Zr (ppm)	0.05677	0.00853	0.06553	0.04089	0.01909	0.02494	0.01278	0.08363	0.02295	0.02637	0.02252	0.00416	0.00301	0.02522	0.00902	0.00251	0.00268	0.01055	5.48E-04	0.01845	8.74E-04	0.00552
Sc (ppm)	45	53	62	61	72	95	97	76	89	97	99	109	104	103	104	105	107	48	52	52	91	90
Al (% - XRF)	3.15	0.52	2.68	2.44	2.6	0.63	0.53	3.25	1.16	0.4	0.32	0.13	0.16	0.31	0.35	0.12	0.13	0.21	0.03	0.43	0.31	1.02
P2O5 (ppm - XRF)	840	90	190	220	715	400	340	420	480	320	330	490	345	460	560	340	590	790	530	350	190	1230

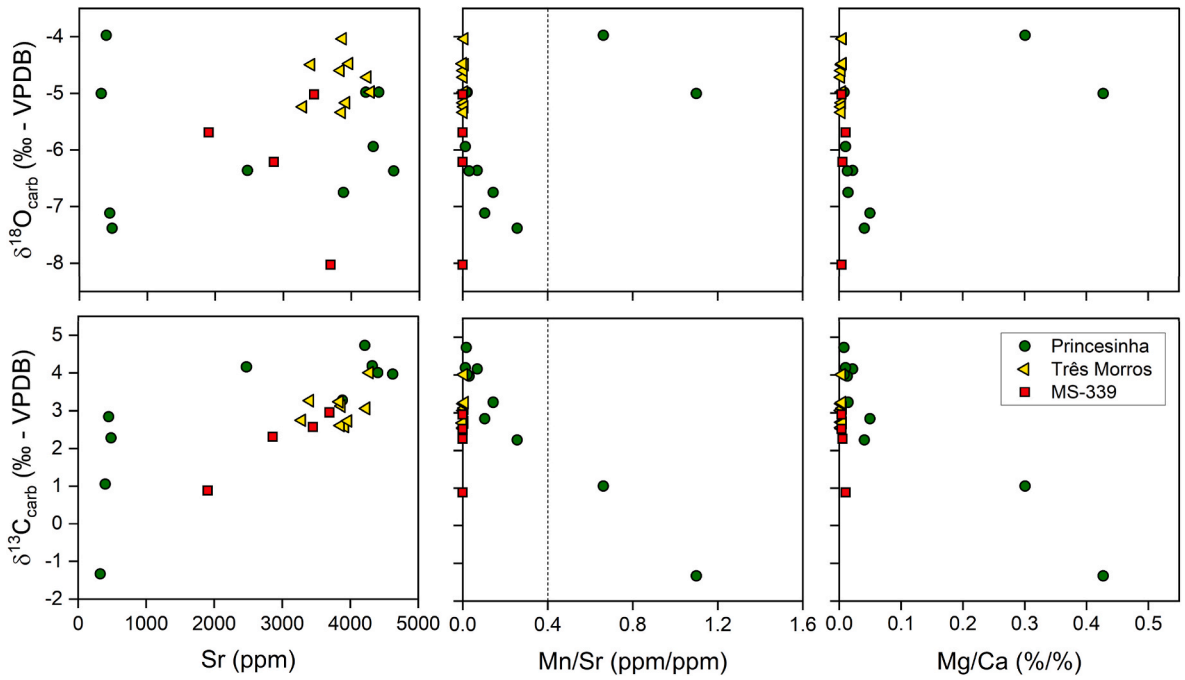

Fig. 8. Bivariate plots of $\delta^{13}C_{carb}$ and $\delta^{18}O_{carb}$ versus Mg/Ca, Mn/Sr and Sr. Note that samples from the lower Princesinha section deviate from other samples in most plots. The dashed lines in 0.4 Mn/Sr indicate the cut-off between altered and unaltered samples. Data is given in Table 1.

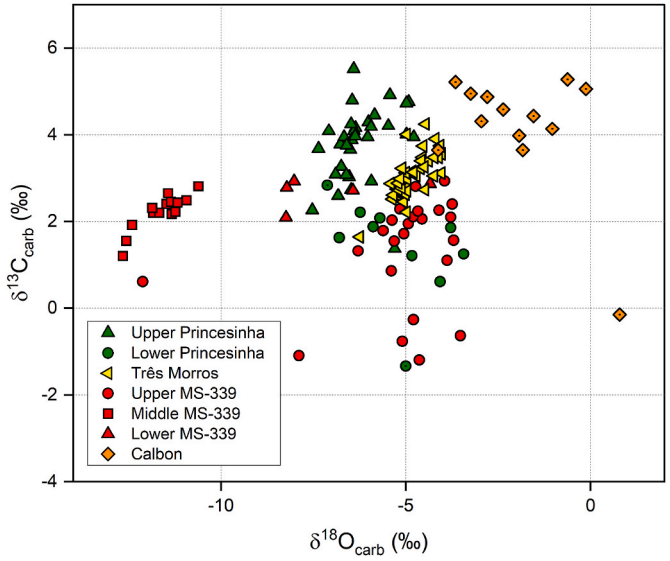

Fig. 9. $\delta^{18}O_{carb}$ versus $\delta^{13}C_{carb}$ bivariate plot of the studied sections. Data of the Calbon section is from Boggiani et al. (2010). Symbols with internal dot represent dolomite samples.

before, supports this interpretation.

5.4. Evaluation of the carbonate leaching method

The efficiency of our leaching method for REY analysis of carbonates was verified through the relationship between ∑REY and the typical detrital indicators Zr, Al, and Sc. There is a significant covariation between ∑REY and Zr ($R^2 = 0.67$), as well as between ∑REY and Al ($R^2 = 0.70$), while there is no significant correlation between ∑REY and Sc ($R^2 = 0.35$) (Fig. 10). Importantly, only samples from the lower Princesinha section showed relatively high Zr and Al concentrations. This suggests that the carbonates from the lower Princesinha section are highly impure, with a possible terrigenous influence on the resulting REY pattern. The samples from the upper Princesinha, Três Morros, Calbon, and MS-339 sections showed considerably low Zr, Al, Sc, and ∑REY, suggesting a successful outcome of the carbonate leaching method.

5.4.1. Origin of REY patterns

Most of the carbonate samples from the Tamengo Formation presented MREE-enriched (MREE-bulge, bell-shaped, or hat-shaped) patterns, as indicated by the MREE/LREE and MREE/HREE ratios. These patterns are similar to previous REY data from the Tamengo Formation in the Corumbá region (Spangenberg et al., 2014), which also presented MREE-enriched patterns in addition to flat distributions. MREE-bulge profiles are commonly documented in pore waters (Haley et al., 2004; Kim et al., 2012) and seawater (Osborne et al., 2015). This enrichment pattern is often derived from complex processes, such as preferential LREE and HREE adsorption by Mn and Fe oxyhydroxides, respectively, resulting in MREE-enriched pore waters (de Baar et al., 1985; Haley et al., 2004; Zhao et al., 2021), preferential LREE and HREE uptake relative to MREE during precipitation of authigenic phosphate (Bryne et al., 1996), preferential MREE adsorption onto Fe–Mn oxyhydroxides in the water column followed by release during reductive dissolution of Fe–Mn oxyhydroxides in pore waters (Haley et al., 2004; Paul et al., 2019; Zhao et al., 2021), and REE complexation with organic matter (Tang and Johannesson, 2010). The ferruginous conditions of the Ediacaran seawater, as mentioned before, and the lack of phosphate minerals in the carbonates of the Tamengo Formation, supports a scenario of preferential uptake of MREE onto Fe–Mn oxyhydroxides and subsequent dissolution, resulting in MREE-enriched pore waters. Afterwards, REE remobilization took place, causing the MREE enrichment in the carbonates. Additionally, organic matter degradation during early diagenesis may have played a minor role on the MREE enrichment process, as sedimentary organic matter also presents MREE-bulge profiles but have about 10 times less REE compared to Fe–Mn nodules (Freslon et al., 2014).

Cerium (Ce) behaves differently compared to other REE. In general, the REE have oxidation number 3+, but in oxidized environments Ce^{3+} is partially oxidized to Ce^{4+}, which does not participate in solid-solution

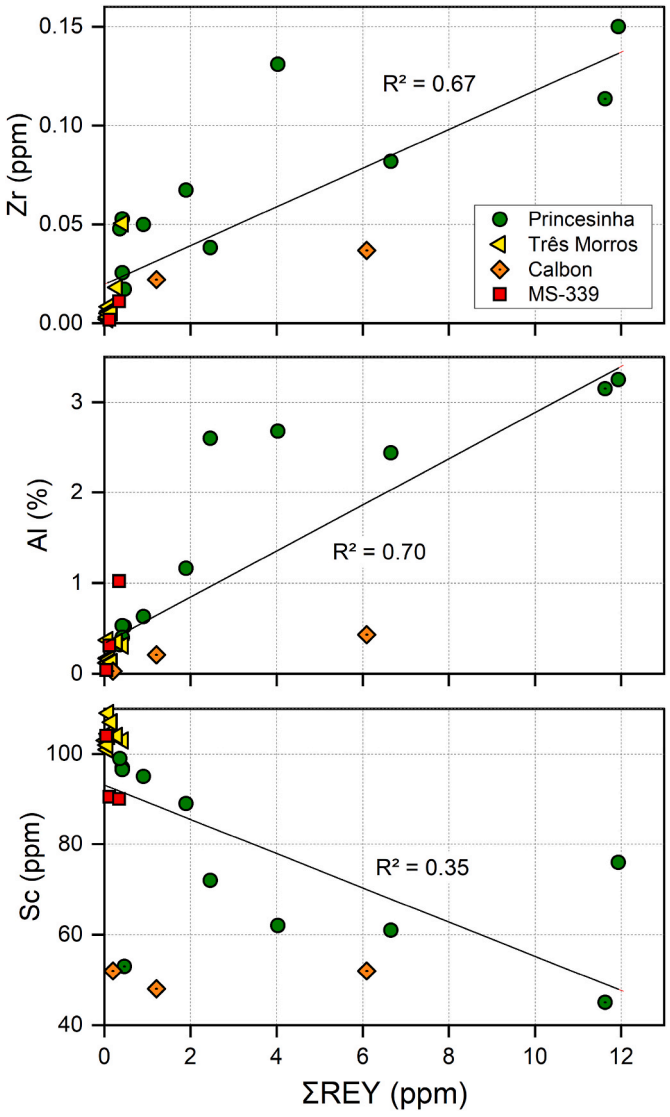

Fig. 10. ∑REY versus Zr, Al, and Sc bivariate plots. Symbols with internal dot represent dolomite samples. Data is given in Table 2.

reactions (Alibo and Nozaki, 1999; German and Elderfield, 1990). As a result, oxygenated waters and carbonates formed in equilibrium with these waters, display a depletion of Ce with respect to the surrounding REE (de Baar et al., 1988), i.e., a negative Ce anomaly. The absence of significant negative Ce anomalies in the rocks of the Tamengo Formation may indicate carbonate precipitation under anoxic water column or diagenetic overprint, which would have caused REY remobilization under anoxic diagenesis (German and Elderfield, 1990; Pattan et al., 2005). The nature of Ce anomalies, if primary or overprinted during diagenesis, may be verified through the correlation of this parameter with post-depositional indicators, such as Dy/Sm, indicative of MREE enrichment, and phosphorus concentration, as precipitation of authigenic phosphate phases may also lead to MREE enrichment (Pattan et al., 2005; Shields and Stille, 2001). There is no significant correlation between $(Ce/Ce^*)_n$ and P_2O_5 (Fig. 11), suggesting a negligible influence of authigenic phosphate on the REY distribution. The $(Ce/Ce^*)_n$ versus $(Dy/Sm)_n$ plot also shows no significant correlation ($R^2 = 0.01$) between the two parameters with respect to the whole dataset. However, when considering only samples from the Princesinha and Três Morros sections, i.e., the sections with the most prominent MREE-bulge patterns and without positive Eu anomalies, a relatively higher covariation ($R^2 = 0.45$) is observed (Fig. 11). This indicates that in the Princesinha and

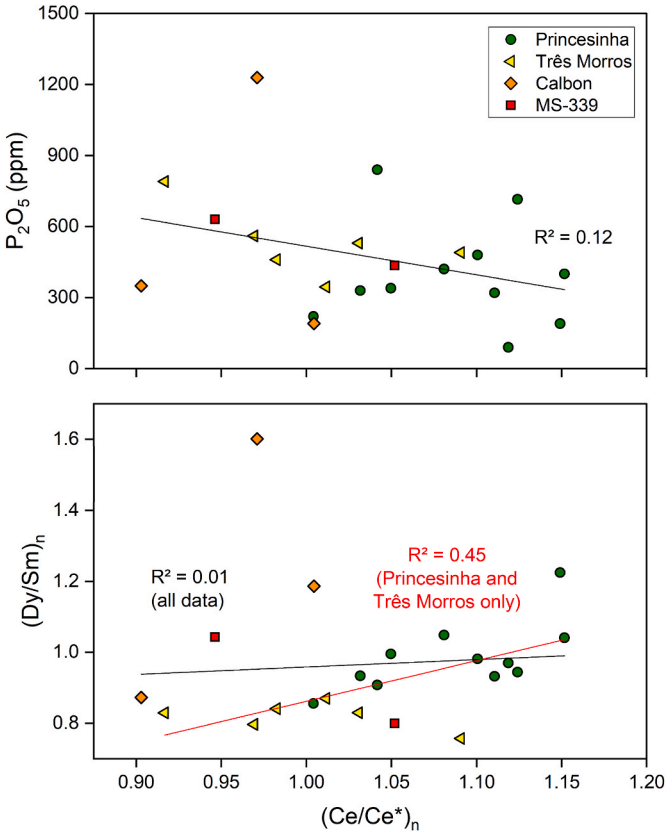

Fig. 11. $(Ce/Ce^*)_n$ versus P_2O_5 and $(Dy/Sm)_n$ bivariate plots. The stronger correlation in the second plot when considering the samples from the Princesinha and Três Morros sections compared to the first plot suggest a diagenetic origin of the Ce anomalies.

Três Morros sections, the Ce anomalies were partially overprinted during early anoxic diagenesis, therefore not serving as a reliable paleoredox proxy in this case.

In the case of the two samples from the MS-339 section, the positive Eu anomaly ($(Eu/Eu^*)_n = 4.2$) and the extremely low values of $\delta^{18}O_{carb}$ strongly suggest that the REY pattern was overprinted during the percolation of high-T fluids, which are enriched in Eu relative to other REY (Bau, 1991). Indeed, the intensity of deformation observed in the MS-339 section is considerably higher compared to other sections, with intrafoliation folds, milonitization, and hydrothermal brecciation supporting this interpretation.

Features typically attributed to the REY "seawater signal" are observed in the REY profiles of the Tamengo Formation, mainly the superchondritic Y/Ho ratios (i.e., Y/Ho > 44) and the positive La anomalies. The relatively high Y/Ho ratios indicate more relative scavenging of Ho compared to Y in the seawater (Bau and Dulski, 1996; Nozaki et al., 1997). Therefore, it is likely that the REY distribution of the carbonate rocks of the Tamengo Formation were partially overprinted during early anoxic diagenesis, resulting in the preservation of some of the original seawater signals, like positive La anomalies and superchondritic Y/Ho ratios, as well as developing MREE-enriched patterns, absent to slightly positive Ce anomalies, and HREE depletion during the diagenetic phase. Samples from the Calbon section may have preserved REY pattern more similar to the original seawater, with minor negative Ce anomalies, high La anomalies and LREE depletion, in a deep water setting.

5.5. Correlations with the Corumbá region and other Gondwana basins

The Tamengo Formation in the Corumbá region is relatively well

constrained in terms of facies (Amorim et al., 2020; Oliveira et al., 2019), geochronology (Parry et al., 2017), biostratigraphy (Adorno et al., 2017) and C isotope chemostratigraphy (Boggiani et al., 2010; Ramos et al., 2022). However, the same unit in the Serra da Bodoquena region (around 200 km south) is poorly constrained in all these fields. Nevertheless, there is a clear stratigraphic correlation between the rocks of the Corumbá Group in both areas (Almeida, 1965). In both localities, the dark limestones of the Tamengo Formation rest above dolomites of the Bocaina Formation, often with a basal polymictic breccia layer (Fernandes et al., 2022), and underlies shales and siltstones of the Guaicurus Formation (Boggiani et al., 2010). The $^{87}Sr/^{86}Sr$ ratios ranging from 0.7083 to 0.7085, verified in both localities (Babinski et al., 2008; Boggiani et al., 2010), are also consistent with the Late Ediacaran $^{87}Sr/^{86}Sr$ values according to the global seawater curve. Thus, despite the lack of geochronological data, the lithostratigraphy seems to be consistent in both Corumbá and Serra da Bodoquena regions, allowing for the correlation of stratigraphic units.

The lowest Tamengo Formation in the Serra da Bodoquena region, i.e., the lower Princesinha section, exhibited only one sample with negative $\delta^{13}C_{carb}$, followed by values around +2 and + 1 ‰. This trend is in relatively good agreement with the lower Tamengo Formation in the type sections of the Laginha and Corcal mines (Boggiani et al., 2010; Ramos et al., 2022), showing that the lower Tamengo Formation is marked by slightly negative to slightly positive values in both Corumbá and Serra da Bodoquena regions. However, the upper Tamengo Formation $\delta^{13}C_{carb}$ record from Corumbá is considerably more positive compared to the data from the Serra da Bodoquena region. Compiled data show that there is a shift of ca. 2 ‰ between the $\delta^{13}C_{carb}$ peaks of both sites (Fig. 12). One possible explanation for this shift is that the sections in Corumbá would represent an overall shallower sector of the carbonate ramp, predominantly above the chemocline and consequently with higher $\delta^{13}C_{carb}$ values (Spangenberg et al., 2014). Indeed, there are no sections of the Tamengo Formation in Corumbá that are interpreted as deep water settings (Amorim et al., 2020). Alternatively, the studied sections in Corumbá and Serra da Bodoquena may have been focused on different time intervals within the deposition of the Tamengo Formation.

Intriguingly, the overall $\delta^{13}C_{carb}$ records in coeval Gondwana carbonate platforms differ greatly, such as the case of the Tamengo Formation (in both Corumbá and Serra da Bodoquena regions, as mentioned above), Itapucumi Group (Paraguay) and Nama Group (Namibia) (Fig. 12). All these records roughly cover the Late Ediacaran ca. 550–538 Ma interval but have $\delta^{13}C_{carb}$ peaks ranging from +2 ‰ (Itapucumi and Nama groups) to +5 ‰ (Tamengo Formation in Corumbá). This difference may be related to latitudinal gradients in the $\delta^{13}C$ of surface seawater DIC, similarly to the modern oceans (Dentith et al., 2020; Murnane and Sarmiento, 2000), or to the degree of basin restriction. The Bambuí Group, for instance, also a Late Ediacaran to Early Cambrian carbonate platform, presents extremely high $\delta^{13}C_{carb}$ (up to +15 ‰) values during the Ediacaran–Cambrian transition due to intense basin restriction and methanogenesis (Caetano-Filho et al., 2021; Cui et al., 2020; Uhlein et al., 2019).

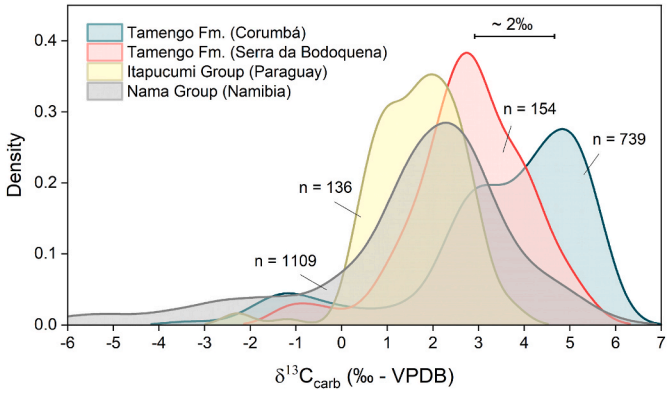

Fig. 12. Density curves of the $\delta^{13}C_{carb}$ data of the Tamengo Formation from Corumbá and Serra da Bodoquena regions, Itapucumi Group, and Nama Group. Data of the Serra da Bodoquena are from this work and Boggiani et al. (2010). Data of Corumbá are compiled from Boggiani et al. (2010), Caetano-Filho (2020), Rivera (2019), and Spangenberg et al. (2014). Data of the Itapucumi Group is from Warren et al. (2017). Data of the Nama Group is from Wood et al. (2015), Bowyer et al. (2022), Saylor et al. (1998), and Smith (1998). Complete dataset is displayed in Table S1.

Notwithstanding the local factors that may influence the value of $\delta^{13}C_{carb}$, shifts in the $\delta^{13}C_{carb}$ of open-marine sections may reflect global changes of the carbon cycle (Bowyer et al., 2022). The values from +3 to +5 ‰ of the studied sections are consistent with the late Ediacaran positive plateau (EPIP; Zhu et al., 2017), after ca. 550 Ma. None of the studied sections present evidence of the Basal Cambrian Negative $\delta^{13}C_{carb}$ Excursion (BACE; Zhu et al., 2006), which suggests that the Tamengo Formation sedimentation did not last until the onset of the BACE, around 539 Ma (Bowyer et al., 2022). In fact, there are no high amplitude carbon isotope excursions documented in the Tamengo Formation upwards, as the magnitude of the $\delta^{13}C_{carb}$ signal remains relatively stable throughout most of the Tamengo Formation carbonate sedimentation around EPIP values. Further high-resolution chemostratigraphy studies must be carried out in order to investigate the complete range of correlative $\delta^{13}C_{carb}$ in the Tamengo Formation.

6. Conclusions

The Tamengo Formation is a key sedimentary succession in the Southern Paraguay Belt that records the environmental and biological changes during the Late Ediacaran. Previous works on the Tamengo Formation focused on its type sections in the Corumbá area. This work extends the investigations on the Tamengo Formation to the Serra da Bodoquena region, approximately 200 km south. The Princesinha, Três Morros, and MS-339 sections show ooid grainstone-dominated successions with wavy, hummocky and swaley cross-stratification interbedded with shales and marls. This facies association is consistent with a storm-dominated carbonate inner to mid-ramp setting. Pyrite framboids are ubiquitous in these sections and their average size points to a mixture of syngenetic and diagenetic framboids under water column shifting from dysoxic to sulfidic.

The isotope record of the Tamengo Formation in the Serra da Bodoquena region is mainly marked by positive values around +3 to +5 ‰ that match the EPIP before the onset of the BACE. Minor short-lived negative excursions linked to facies variations and a regional trend in decreasing average $\delta^{13}C_{carb}$ from west to east are consistent with a C isotope depth gradient, resulted from seawater redox stratification that led to a large DOC pool in bottom waters and subsequent ^{13}C-depleted DIC. There is a shift of approximately 2 ‰ between the Tamengo Formation $\delta^{13}C_{carb}$ record from Corumbá and Serra da Bodoquena regions. This offset may be linked to either differences on the predominant ramp sector of each locality or to different temporal constraints. The overall $\delta^{13}C_{carb}$ of the Tamengo Formation also differs from other coeval Gondwana basins, such as the Nama and Itapucumi groups, which may be related to latitudinal differences on the C isotope composition of DIC or to the degree of basin restriction.

Most of the rare earth elements and yttrium profiles of the carbonates of the Tamengo Formation display a MREE-bulge pattern, associated with preferential MREE adsorption onto Fe–Mn oxyhydroxides and subsequent release in pore waters, where REY remobilization took place. In this case, the samples from the Tamengo Formation record some of the original seawater signals, such as positive La anomalies and superchondritic Y/Ho ratios, as well as early anoxic diagenetic processes, represented by the MREE-bulge pattern and the absent to slightly positive Ce anomalies.

CRediT authorship contribution statement

Henrique Albuquerque Fernandes: Writing – review & editing, Writing – original draft, Methodology, Investigation, Conceptualization. **Paulo César Boggiani:** Writing – review & editing, Resources, Project administration, Conceptualization. **Aghata Zarelli Viana:** Writing – review & editing, Investigation, Conceptualization. **Sergio Caetano-Filho:** Writing – review & editing, Methodology. **Luiz Gustavo Pereira:** Writing – review & editing. **Bernardo Freitas:** Writing – review & editing, Conceptualization. **João Pedro Hippertt:** Writing – review & editing, Conceptualization. **Luana Morais:** Writing – review & editing. **Ricardo Ivan Ferreira Trindade:** Writing – review & editing, Project administration, Funding acquisition.

Declaration of competing interest

The authors declare that they have no known competing financial interests or personal relationships that could have appeared to influence the work reported in this paper.

Data availability

Data is provided in tables

Acknowledgements

We would like to acknowledge the São Paulo Research Foundation (FAPESP) for funding this project (grants 2021/02628–3, 2020/16140–0 and 2016/06114–6). PCB and RIT are fellows of the Brazilian National Council for Scientific and Technological Development (CNPq). We also thank EDEM Agrominerais and Prospecção Minerária Rio Miranda LTDA for their support during the field works.

Appendix A. Supplementary data

Supplementary data to this article can be found online at https://doi.org/10.1016/j.jsames.2023.104696.

References

Adorno, R.R., do Carmo, D.A., Germs, G., Walde, D.H.G., Denezine, M., Boggiani, P.C., Sousa e Silva, S.C., Vasconcelos, J.R., Tobias, T.C., Guimarães, E.M., Vieira, L.C., Figueiredo, M.F., Moraes, R., Caminha, S.A., Suarez, P.A.Z., Rodrigues, C.V., Caixeta, G.M., Pinho, D., Schneider, G., Muyamba, R., 2017. Cloudina lucianoi (Beurlen & sommer, 1957), Tamengo Formation, ediacaran. Precambrian Res. 301, 19–35. https://doi.org/10.1016/j.precamres.2017.08.023. Brazil: Taxonomy, analysis of stratigraphic distribution and biostratigraphy.

Alibo, D.A., Nozaki, Y., 1999. Rare earth elements in seawater: particle association, shale-normalization, and Ce oxidation. Geochem. Cosmochim. Acta 63 (3–4), 363–372. https://doi.org/10.1016/S0016-7037(98)00279-8.

Allan, J.R., Matthews, R.K., 1982. Isotope signatures associated with early meteoric diagenesis. Sedimentology 29, 797–817.

Almeida, F.F.M., 1965. Geologia da Serra da Bodoquena (Mato Grosso). DNPM.

Alvarenga, C., Trompette, R., 1993. Evolução tectônica brasiliana da Faixa Paraguai: a estruturação da região de Cuiabá. Rev. Bras. Geociencias 23, 18–30. https://doi.org/10.25249/0375-7536.19932311830.

Alvarenga, C.J.S., Boggiani, P.C., Babinski, M., Dardenne, M.A., Figueiredo, M., Santos, R.V., Dantas, E.L., 2010. Chapter 2 the amazonian palaeocontinent. Dev. Precambrian Geol., 01602 https://doi.org/10.1016/S0166-2635(09).

Alvarenga, C.J.S., Boggiani, P.C., Babinski, M., Dardenne, M.A., Figueiredo, M.F., Dantas, E.L., Uhlein, A., Santos, R.V., Sial, A.N., Trompette, R., 2011. Glacially influenced sedimentation of the Puga Formation, Cuiabá group and Jacadigo group, and associated carbon- ates of the araras and Corumbá groups, Paraguay belt, Brazil. In: Arnaud, E., Halverson, G.P., Shields-Zhou, G. (Eds.), The Geological Record of Neoproterozoic Glaciations. Geological Society, London, Memoirs, pp. 487–497. https://doi.org/10.1144/M36.45, 36.

Amorim, K.B., Afonso, J.W.L., Leme, J., de M, Diniz, C.Q.C., Rivera, L.C.M., Gómez-Gutiérrez, J.C., Boggiani, P.C., Trindade, R.I.F., 2020. Sedimentary facies, fossil distribution and depositional setting of the late Ediacaran Tamengo Formation (Brazil). Sedimentology 67, 3422–3450. https://doi.org/10.1111/sed.12749.

Árting, T.B., Boggiani, P.C., Gaucher, C., Fernandes, H.A., Frei, R., 2023. Strong positive fractionation of chromium isotopes in iron formation of the Jacadigo Group (Brazil)-A link to enhanced atmospheric oxygenation during the Late Neoproterozoic. Gondwana Res. 124, 39–60. https://doi.org/10.1016/j.gr.2023.06.017.

Babinski, M., Boggiani, P.C., Fanning, C.M., Fairchild, T.R., Simon, C.M., Sial, A.N., 2008. U-Pb shrimp geochronology and isotope chemostratigraphy (C, O, Sr) of the Tamengo Formation, southern Paraguay belt. In: VI South American Symposium on Isotope Geology. Book of Abstracts, San Carlos de Bariloche, Brazil, p. 160.

Babinski, M., Boggiani, P.C., Trindade, R.I.F., Fanning, C.M., 2013. Detrital zircon ages and geochronological constraints on the Neoproterozoic Puga diamictites and associated BIFs in the southern Paraguay Belt, Brazil. Gondwana Res. 23, 988–997. https://doi.org/10.1016/j.gr.2012.06.011.

Banner, J.L., Hanson, G.N., 1990. Calculation of simultaneous isotopic and trace element variations during wate-rock interaction with applications to carbonate diagenesis. Geochem. Cosmochim. Acta 54 (1), 3123–3137. https://doi.org/10.1016/0016-7037(90)90128-8.

Bau, M., 1991. Rare-earth element mobility during hydrothermal and metamorphic fluid-rock interaction and the significance of the oxidation state of europium. Chem. Geol. 93 (3–4), 219–230. https://doi.org/10.1016/0009-2541(91)90115-8.

Bau, M., Dulski, P., 1996. Distribution of yttrium and rare-earth elements in the penge and kuruman iron-formations, transvaal supergroup, South Africa. Precambrian Res. 79, 37–55. https://doi.org/10.1016/0301-9268(95)00087-9.

Becker-Kerber, B., Elmola, A.A., Zhuravlev, A., Gaucher, C., Simões, M.G., Prado, G.M.E. M., Vintaned, J.A.G., Fontaine, C., Lino, L.M., Sanchez, D.F., Galante, D., Paim, P.S. G., Callefo, F., Kerber, G., Meunier, A., El Albani, A., 2022. Clay templates in Ediacaran vendotaeniaceans: implications for the taphonomy of carbonaceous fossils. Bull. Geol. Soc. Am. 134, 1334–1346. https://doi.org/10.1130/B36033.1.

Becker-Kerber, B., Pacheco, M.L.A.F., Rudnitzki, I.D., Galante, D., Rodrigues, F., Leme, J. D.M., 2017. Ecological interactions in Cloudina from the Ediacaran of Brazil: implications for the rise of animal biomineralization. Sci. Rep. 7 (5842) https://doi.org/10.1038/s41598-017-05753-8.

Bjerrum, C.J., Canfield, D.E., 2011. Towards a quantitative understanding of the late Neoproterozoic carbon cycle. Proc. Natl. Acad. Sci. U.S.A. 108, 5542–5547. https://doi.org/10.1073/pnas.1101755108.

Blood, D.R., Schlaegle, S., Hefferan, C.M., Vazquez, A., McAllister, D., 2020. Diagenetic pyrite morphology in mudstones of the upper ordovician point pleasant limestone, appalachian basin: evidence for dysoxic deposition. In: Memoir 120: Mudstone Diagenesis: Research Perspectives for Shale Hydrocarbon Reservoirs, Seals, and Source Rocks, pp. 69–82. https://doi.org/10.1306/13672211m1213822.

Boddy, C.E., Mitchell, E.G., Merdith, A., Liu, A.G., 2022. Palaeolatitudinal distribution of the Ediacaran macrobiota. J. Geol. Soc. 179 https://doi.org/10.1144/jgs2021-030.

Boggiani, P.C., 1998. Análise Estratigráfica da Bacia Corumbá (Neoproterozóico) - Mato Grosso do Sul. Universidade de São Paulo, São Paulo. PhD Thesis.

Boggiani, P.C., Gaucher, C., Sial, A.N., Babinski, M., Simon, C.M., Riccomini, C., Ferreira, V.P., Fairchild, T.R., 2010. Chemostratigraphy of the Tamengo Formation (Corumbá group, Brazil): a contribution to the calibration of the ediacaran carbon-isotope curve. Precambrian Res. 182 (4), 382–401. https://doi.org/10.1016/j.precamres.2010.06.003.

Boggiani, P.C., Ferreira, V.P., Sial, A.N., Babinski, M., Trindade, R.I.F., Acenolaza, G., Toselli, A.J., Parada, M.A., 2003. The cap carbonate of the Puga hill (central south America) in the context of the post-varanger glaciation. In: IV south American symposium on isotope geology,. Abstracts 1, 324–327.

Bowyer, F., Wood, R.A., Poulton, S.W., 2017. Controls on the evolution of Ediacaran metazoan ecosystems: a redox perspective. Geobiology 15, 516–551. https://doi.org/10.1111/gbi.12232.

Bowyer, F.T., Zhuravlev, A.Y., Wood, R., Shields, G.A., Zhou, Y., Curtis, A., Poulton, S. W., Condon, D.J., Yang, C., Zhu, M., 2022. Calibrating the temporal and spatial dynamics of the Ediacaran - Cambrian radiation of animals. Earth Sci. Rev. 225, 103913 https://doi.org/10.1016/j.earscirev.2021.103913.

Brand, U., Veizer, J., 1980. Chemical diagenesis of a multicomponent carbonate system; 1, Trace elements. J. Sediment. Res. 50 (4), 1219–1236. https://doi.org/10.1306/212F7BB7-2B24-11D7-8648000102C1865D.

Bryne, R.H., Liu, X., Schijf, J., 1996. The influence of phosphate coprecipitation on rare earth distributions in natural waters. Geochem. Cosmochim. Acta 60 (17), 3341–3346. https://doi.org/10.1016/0016-7037(96)00197-4.

Burchette, T.P., Wright, V.P., 1992. Carbonate ramp depositional systems. Sediment. Geol. 79, 3–57. https://doi.org/10.1016/0037-0738(92)90003-A.

Caetano-Filho, S., Sansjofre, P., Ader, M., Paula-Santos, G.M., Guacaneme, C., Babinski, M., Bedoya-Rueda, C., Kuchenbecker, M., Reis, H.L.S., Trindade, R.I.F., 2021. A large epeiric methanogenic Bambuí sea in the core of Gondwana supercontinent? Geosci. Front. 12 (1), 203–218. https://doi.org/10.1016/j.gsf.2020.04.005.

Caetano-Filho, S., 2020. C and S Biogeochemical Cycles in the Brazilian Ediacaran Record. Universidade de São Paulo, São Paulo. PhD Thesis.

Campanha, G.A., Boggiani, P.C., Filho, W.S., Sá, F.R., Zuquim, M., Piacentini, T., 2011. The Paraguay Fold Belt in the Serra da Bodoquena and Miranda River Depression, Mato Grosso do sul. Geol. Usp. Série Científica 11, 79–96. https://doi.org/10.5327/z1519-874x2011000300005.

Canfield, D.E., Poulton, S.W., Knoll, A.H., Narbonne, G.M., Ross, G., Goldberg, T., Strauss, H., 2008. Ferruginous conditions dominated later Neoproterozoic deep-water chemistry. Science 321, 949–952.

Carvalho, D.F., Nogueira, A.C.R., Macambira, M.J.B., Lana, C.C., Santos, R.F., Guélard, J., Sansjofre, P., 2023. Constraining the diagenesis of the Puga cap carbonate from U–Pb in-situ dating of seafloor crystal fans, southern Amazonian craton. Brazil. Terra Nova 35 (4), 276–284. https://doi.org/10.1111/ter.12652.

Caxito, F., Lana, C., Frei, R., Uhlein, G.J., Sial, A.N., Dantas, E.L., Pinto, A.G., Campos, F. C., Galvão, P., Warren, L.V., Okubo, J., Ganade, C.E., 2021. Goldilocks at the dawn of complex life: mountains might have damaged Ediacaran–Cambrian ecosystems and prompted an early Cambrian greenhouse world. Sci. Rep. 11, 1–15. https://doi.org/10.1038/s41598-021-99526-z.

Caxito, F., de A, Uhlein, G.J., Uhlein, A., Pedrosa-Soares, A.C., Kuchenbecker, M., Reis, H., Sial, A.N., Ferreira, V.P., Alvarenga, C.J.S., Santos, R.V., Vieira, L.C., Dantas, E., Babinski, M., Trindade, R., Boggiani, P.C., Warren, L., Hippertt, J.P., Sotero, M.P., Rodrigues de Paula, J., 2019. Isotope stratigraphy of Precambrian sedimentary rocks from Brazil: Keys to unlock Earth's hydrosphere, biosphere, tectonic, and climate evolution 73–132. https://doi.org/10.1016/bs.sats.2019.08.002.

Cordani, U.G., Fairchild, T.R., Ganade, C.E., Babinski, M., Leme, J.M., 2020. Dawn of metazoans: to what extent was this influenced by the onset of "modern-type plate tectonics"? Braz. J. Genet. 50 (2), e20190095 https://doi.org/10.1590/2317-4889202020190095.

Cui, H., Warren, L.V., Uhlein, G.J., Okubo, J., Liu, X.M., Plummer, R.E., Baele, J.M., Goderis, S., Claeys, P., Li, F., 2020. Global or regional? Constraining the origins of the middle Bambuí carbon cycle anomaly in Brazil. Precambrian Res. 348 (15), 105861 https://doi.org/10.1016/j.precamres.2020.105861.

De Baar, H.J.W., Brewer, P.G., Bacon, M.P., 1985. Anomalies in rare earth distributions in seawater: Gd and Tb. Geochem. Cosmochim. Acta 49 (9), 1961–1969. https://doi.org/10.1016/0016-7037(85)90090-0.

De Baar, H.J.W., German, C.R., Elderfield, H., van Gaans, P., 1988. Rare earth element distributions in anoxic waters of the Cariaco Trench. Geochem. Cosmochim. Acta 52 (5), 1203–1219. https://doi.org/10.1016/0016-7037(88)90275-X.

D'el-Rey Silva, Walde, L.J.H., Dhg, Saldanha, D.O., 2016. The Neoproterozoic–Cambrian Paraguay Belt, central Brazil: Part I — new structural data and a new approach on the regional implications. Tectonophysics 676, 20–41. https://doi.org/10.1016/J.TECTO.2016.03.019.

Dentith, J.E., Ivanovic, R.F., Gregoire, L.J., Tindall, J.C., Robinson, L.F., 2020. Simulating stable carbon isotopes in the ocean component of the FAMOUS general circulation model with MOSES1 (XOAVI). Geosci. Model Dev. (GMD) 13, 3529–3552. https://doi.org/10.5194/GMD-13-3529-2020.

Dias-Brito, D., 2017. Guia petrográfico dos carbonatos do Brasil. Rio Claro: UNESP, IGCE-UNESPetro. Obra 4.

Dickson, J.A.D., 1966. Carbonate identification and genesis as revealed by staining. J. Sediment. Res. 36 (2), 491–505. https://doi.org/10.1306/74D714F6-2B21-11D7-8648000102C1865D.

Diniz, C.Q.C., Leme, J., de M, Boggiani, P.C., 2021. New species of macroalgae from Tamengo Formation, ediacaran, Brazil. Front. Earth Sci. 9, 1–11. https://doi.org/10.3389/feart.2021.748876.

Dott, R.H., Bourgeois, J., 1982. Hummocky cross- stratification: significance of its variable bedding sequences. Bull. Geol. Soc. Am. 93, 663–680.

Droser, M.L., Tarhan, L.G., Gehling, J.G., 2017. The rise of animals in a changing environment: global ecological innovation in the late ediacaran. Annual Rev. 45, 593–617. https://doi.org/10.1146/ANNUREV-EARTH-063016-015645.

Dumas, S., Arnott, R.W.C., 2006. Origin of hummocky and swaley cross-stratification–The controlling influence of unidirectional current strength and aggradation rate. Geology 34, 1073–1076.

Fazio, G., Guimarães, E.M., Walde, D.W.G., do Carmo, D.A., Adorno, R.R., Vieira, L.C., Denezine, M., Silva, C.B. da, Godoy, H.V. de, Borges, P.C., Pinho, s, 2019. Mineralogical and chemical composition of Ediacaran-Cambrian pelitic rocks of the Tamengo and Guaicurus formations, (Corumbá Group - MS, Brazil): stratigraphic positioning and paleoenvironmental interpretations. J. S. Am. Earth Sci. 90, 487–503. https://doi.org/10.1016/j.jsames.2018.11.025.

Fernandes, H.A., Boggiani, P.C., Afonso, J.W.L., Amorim, K.B., Trindade, R.I.F., 2022. Sedimentary and tectonic breccias at the base of the ediacaran Tamengo Formation (Corumbá group): a comparative study. Braz. J. Genet. 52 https://doi.org/10.1590/2317-4889202220210062.

Font, E., Nédélec, A., Trindade, R.I.F., Macouin, M., Charrière, A., 2006. Chemostratigraphy of the Neoproterozoic Mirassol d'Oeste cap dolostones (Mato Grosso, Brazil): an alternative model for Marinoan cap dolostone formation. Earth Planet Sci. Lett. 250, 89–103. https://doi.org/10.1016/j.epsl.2006.06.047.

Frei, R., Døssing, L.N., Gaucher, C., Boggiani, P.C., Frei, K.M., Bech Árting, T., Crowe, S. A., Freitas, B.T., 2017. Extensive oxidative weathering in the aftermath of a late Neoproterozoic glaciation – evidence from trace element and chromium isotope records in the Urucum district (Jacadigo Group) and Puga iron formations (Mato Grosso do Sul, Brazil). Gondwana Res. 49, 1–20. https://doi.org/10.1016/j.gr.2017.05.003.

Frei, R., Gaucher, C., Stolper, D., Canfield, D.E., 2013. Fluctuations in late Neoproterozoic atmospheric oxidation — Cr isotope chemostratigraphy and iron speciation of the late Ediacaran lower Arroyo del Soldado Group (Uruguay). Gondwana Res. 23, 797–811. https://doi.org/10.1016/J.GR.2012.06.004.

Freitas, B.T., Rudnitzki, I.D., Morais, L., Campos, M.D.R., Almeida, R.P., Warren, L.V., Boggiani, P.C., Caetano-Filho, S., Bedoya-Rueda, C., Babinski, M., Fairchild, T.R., Trindade, R.I.F., 2021. Cryogenian glaciostatic and eustatic fluctuations and massive Marinoan-related deposition of Fe and Mn in the Urucum District, Brazil. Geology 49, 1478–1483. https://doi.org/10.1130/G49134.1.

Freitas, B.T., Warren, L.V., Boggiani, P.C., De Almeida, R.P., Piacentini, T., 2011. Tectono-sedimentary evolution of the neoproterozoic BIF-bearing Jacadigo group, SW-Brazil. Sediment. Geol. 238 (1–2), 48–70. https://doi.org/10.1016/j.sedgeo.2011.04.001.

Freslon, N., Bayon, G., Toucanne, S., Bermell, S., Bollinger, C., Chéron, S., Etoubleau, J., Germain, Y., Khripounoff, A., Ponzevera, E., Rouget, M.L., 2014. Rare earth elements and neodymium isotopes in sedimentary organic matter. Geochem. Cosmochim. Acta 140, 177–198. https://doi.org/10.1016/j.gca.2014.05.016.

Gaucher, C., Boggiani, P.C., Sprechmann, P., Sial, A.N., Fairchild, T., 2003. Integrated correlation of the Vendian to Cambrian Arroyo del Soldado and Corumbá Groups (Uruguay and Brazil): palaeogeographic, palaeoclimatic and palaeobiologic implications. Precambrian Res. 120, 241–278. https://doi.org/10.1016/S0301-9268(02)00140-7.

German, C.R., Elderfield, H., 1990. Application of the Ce anomaly as a paleoredox indicator: the ground rules. Paleoceanography 5 (5), 823–833. https://doi.org/10.1029/PA005i005p00823.

Giddings, J.A., Wallace, M.W., 2009. Facies-dependent $\delta^{13}C$ variation from a cryogenian platform margin, south Australia: evidence for stratified neoproterozoic oceans? Palaeogeography, palaeoclimatology. Palaeoecology 271 (3–4), 196–214. https://doi.org/10.1016/j.palaeo.2008.10.011.

Hahn, G., Hahn, R., Leonardos, O.H., Pflug, H.D., 1982. Kfrperlich erhaltene Scyphozoenreste aus dem Jungprekambrium Brasiliens. Geologika et Paleontologica 16, 1–18.

Hahn, G., Pflug, H.D., 1985. Die cloudinidae n. farm., Kalk-Rfhren aus dem Vendium und Unter-Kambrium. Senckenbergiana 65, 413–431.

Haley, B.A., Klinkhammer, G.P., McManus, J., 2004. Geochimica et. Cosmochimica Acta 68 (6), 1265–1279. https://doi.org/10.1016/j.gca.2003.09.012.

Hayes, J.M., Strauss, H., Kaufman, A.J., 1999. The abundance of 13C in marine organic matter and isotopic fractionation in the global biogeochemical cycle of carbon during the past 800 Ma. Chem. Geol. 161, 103–125. https://doi.org/10.1016/S0009-2541(99)00083-2.

Hiatt, E.E., Pufahl, P.K., Guimarães da Silva, L., 2020. Iron and Phosphorus Biochemical Systems and the Cryogenian-Ediacaran Transition. Implications for the Neoproterozoic oxygenation event, Jacadigo basin, Brazil. https://doi.org/10.1016/j.precamres.2019.105533. Precambrian Research, 337, 105533.

Hippertt, J.P.T.M., Rudnitzki, I.D., Morais, L., Freitas, B., Romero, G.R., Fernandes, H.A., Leite, M.G.P., Leme, J.M., Boggiani, P.C., Trindade, R.I.F., 2023. Sedimentary evolution and sequence stratigraphy of Ediacaran high-grade phosphorite–dolomite–shale successions of the Bocaina Formation (Corumbá Group), Central Brazil: implications for the Neoproterozoic phosphogenic event. Sedimentology. https://doi.org/10.1111/sed.13125.

Jacobsen, S.B., Kaufman, A.J., 1999. The Sr, C and O isotopic evolution of Neoproterozoic seawater. Chem. Geol. 161, 37–57. https://doi.org/10.1016/S0009-2541(99)00080-7.

Jiang, G., Kaufman, A.J., Christie-Blick, N., Zhang, S., Wu, H., 2007. Carbon isotope variability across the Ediacaran Yangtze platform in South China: implications for a large surface-to-deep ocean $\delta^{13}C$ gradient. Earth Planet Sci. Lett. 261 (1–2), 303–320. https://doi.org/10.1016/j.epsl.2007.07.009.

Johnston, D.T., MacDonald, F.A., Gill, B.C., Hoffman, P.F., Schrag, D.P., 2012. Uncovering the neoproterozoic carbon cycle. Nature 483, 320–323. https://doi.org/10.1038/nature10854.

Kaufman, A.J., Knoll, A.H., 1995. Neoproterozoic variations in the C-isotopic composition of seawater: stratigraphic and biogeochemical implications. Precambrian Res. 73 (1–4), 27–49. https://doi.org/10.1016/0301-9268(94)00070-8.

Kim, J.H., Torres, M.E., Haley, B.A., Kastner, M., Pohlman, J.W., Riedel, M., Lee, Y.J., 2012. The effect of diagenesis and fluid migration on rare earth element distribution in pore fluids of the northern Cascadia accretionary margin. Chem. Geol. 291, 152–165. https://doi.org/10.1016/j.chemgeo.2011.10.010.

Laakso, T.A., Schrag, D.P., 2020. The role of authigenic carbonate in Neoproterozoic carbon isotope excursions. Earth Planet Sci. Lett. 549, 116534 https://doi.org/10.1016/j.epsl.2020.116534.

Labaj, M.A., Pratt, B.R., 2016. Depositional dynamics in a mixed carbonate-siliciclastic system: Middle-Upper Cambrian Abrigo Formation, southeastern Arizona, U.S.A. J. Sediment. Res. 86, 11–37.

Lawrence, M.G., Greig, A., Collerson, K.D., Kamber, B.S., 2006. Rare earth element and yttrium variability in South East Queensland waterways. Aquat. Geochem. 12, 39–72.

Leme, J.M., Van Iten, H., Simões, M.G., 2022. A New Conulariid (Cnidaria, Scyphozoa) From the Terminal Ediacaran of Brazil. Frontiers in Earth Science 10. https://doi.org/10.3389/feart.2022.777746.

Li, C., Love, G.D., Lyons, T.W., Fike, D.A., Sessions, A.L., Chu, X., 2010. A stratified redox model for the Ediacaran Ocean. Science 328 (5974), 80–83. https://doi.org/10.1126/science.118236.

Maciel, P., 1959. Tilito Cambriano no Estado de Mato Grosso. Boletim Soc. Bras. Geol. 8, 31–39.

Manzano, J.C., Godoy, A.M., de Araújo, L.M.B., 2008. Contexto tectônico dos granitóides neoproterozóicos da faixa de dobramentos paraguai, MS e MT. Geociencias 27, 493–507.

McGee, B., Babinski, M., Trindade, R., Collins, A.S., 2018. Tracing final Gondwana assembly: Age and provenance of key stratigraphic units in the southern Paraguay Belt, Brazil. Precambrian Res. 307, 1–33. https://doi.org/10.1016/j.precamres.2017.12.030.

Mills, D.B., Canfield, D.E., 2014. Oxygen and animal evolution: Did a rise of atmospheric oxygen "trigger" the origin of animals? Bioessays 36, 1145–1155. https://doi.org/10.1002/bies.201400101.

Morais, L., Fairchild, T.R., Freitas, B.T., Rudnitzki, I.D., Silva, E.P., Lahr, D., Moreira, A. C., Abrahão Filho, E.A., Leme, J.M., Trindade, R.I.F., 2021. Doushantuo-Pertatataka—Like Acritarchs from the Late Ediacaran Bocaina Formation (Corumbá Group, Brazil). Front. Earth Sci. 9 https://doi.org/10.3389/feart.2021.787011.

Murnane, R.J., Sarmiento, J.L., 2000. Roles of biology and gas exchange in determining the $\delta^{13}C$ distribution in the ocean and the preindustrial gradient in atmospheric $\delta^{13}C$. Global Biogeochem. Cycles 14 (1), 389–405. https://doi.org/10.1029/1998GB001071.

Nogueira, A.C.R., Riccomini, C., Sial, A.N., Moura, C.A.V., Fairchild, T.R., 2003. Soft-sediment deformation at the base of the Neoproterozoic Puga cap carbonate (southwestern Amazon craton, Brazil): Confirmation of rapid icehouse to greenhouse

transition in snowball Earth. Geology 31 (7), 613–616. https://doi.org/10.1130/0091-7613(2003)031<0613:SDATBO>2.0.CO;2.
Nogueira, A.C.R., Santos, R.F., Romero, G.R., Bandeira, J., Riccomini, C., Barrera, I.A.R., Silva, P.A.S., Soares, J.L., Fairchild, T.R., Nogueira, A.A.E., Góes, A.M., Oliveira, R. S., Medeiros, R.S.P., Andrade, L.S., Brito, A.S., Oliveira, P.G.A., Sodré, A.A.N., Carvalho, D.F., Truckenbrodt, W., 2022. Ediacaran-Cambrian microbialites of the Southern Amazon Craton: relation with the metazoan rise, sea-level changes, and global tectonics. Braz. J. Genet. 52 (2) https://doi.org/10.1590/2317-4889202220210065.
Nozaki, Y., Zhang, J., Amakawa, H., 1997. The fractionation between Y and Ho in the marine environment. Earth Planet Sci. Lett. 148, 329–340. https://doi.org/10.1016/S0012-821X(97)00034-4.
Och, L.M., Shields-Zhou, G.A., 2012. The Neoproterozoic oxygenation event: Environmental perturbations and biogeochemical cycling. Earth Sci. Rev. 110, 26–57. https://doi.org/10.1016/j.earscirev.2011.09.004.
Oliveira, R.S., Nogueira, A.C.R., Romero, G.R., Truckenbrodt, W., Bandeira, J.C.S., 2019. Ediacaran ramp depositional model of the Tamengo Formation, Brazil. J. S. Am. Earth Sci. 96, 102348 https://doi.org/10.1016/j.jsames.2019.102348.
Osborne, A.H., Haley, B.A., Hathorne, E.C., Plancherel, Y., Frank, M., 2015. Rare earth element distribution in Caribbean seawater: Continental inputs versus lateral transport of distinct REE compositions in subsurface water masses. Mar. Chem. 177, 172–183. https://doi.org/10.1016/J.MARCHEM.2015.03.013.
Parry, L.A., Boggiani, P.C., Condon, D.J., Garwood, R.J., Leme, J.D.M., McIlroy, D., Brasier, M.D., Trindade, R., Campanha, G.A.C., Pacheco, M.L.A.F., Diniz, C.Q.C., Liu, A.G., 2017. Ichnological evidence for meiofaunal bilaterians from the terminal Ediacaran and earliest Cambrian of Brazil. Nat. Ecol. Evol. 1, 1455–1464. https://doi.org/10.1038/s41559-017-0301-9.
Pattan, J.N., Pearce, N.J.G., Mislankar, P.G., 2005. Constraints in using Cerium-anomaly of bulk sediments as indicator of paleo bottom water redox environment: A case study from the Central Indian Ocean Basin. Chem. Geol. 221 (3–4), 260–278. https://doi.org/10.1016/j.chemgeo.2005.06.009.
Paul, S.A.L., Haeckel, M., Bau, M., Bajracharya, R., Koschinsky, A., 2019. Small-scale heterogeneity of trace metals including rare earth elements and yttrium in deep-sea sediments and porewaters of the Peru Basin, southeastern equatorial Pacific. Biogeosciences 16 (24), 4829–4849. https://doi.org/10.5194/bg-16-4829-2019.
Paula-Santos, G.M., Caetano-Filho, S., Enzweiler, J., Navarro, M.S., Babinski, M., Guacaneme, C., Kuchenbecker, M., Reis, H., Trindade, R.I.F., 2020. Rare earth elements in the terminal Ediacaran Bambuí Group carbonate rocks (Brazil): evidence for high seawater alkalinity during rise of early animals. Precambrian Res. 336, 105506 https://doi.org/10.1016/j.precamres.2019.105506.
Pourmand, A., Dauphas, N., Ireland, T.J., 2012. A novel extraction chromatography and MC-ICP-MS technique for rapid analysis of REE, Sc and Y: Revising CI-chondrite and Post-Archean Australian Shale (PAAS) abundances. Chem. Geol. 291, 38–54. https://doi.org/10.1016/j.chemgeo.2011.08.011.
Ramos, M.E.A.F., Giorgioni, M., Walde, D.H.G., Carmo, D.A., Fazio, G., Vieira, L.C., Denezine, M., Santos, R.V., Adorno, R.R., Guida, L.L., 2022. New facies model and carbon isotope stratigraphy for and Ediacaran carbonate platform from South America (Tamengo Formation – Corumbá Group, SW Brazil). Front. Earth Sci. 10, 749066 https://doi.org/10.3389/feart.2022.749066.
Reading, H.G., 1996. Sedimentary Environments: Process. In: Facies and Stratigraphy, third ed. Blackwell, Oxford, p. 629.
Rivera, L.C.M., 2019. C and O Isotopes of the Middle and Upper Tamengo Formation (Corumbá Group- Upper Ediacaran): Effects of the Sedimentary Facies and Diagenesis. Universidade de São Paulo, São Paulo. MSc Dissertation.
Romero, G.R., Sanchez, E.A.M., Morais, L., Boggiani, P.C., Fairchild, T.R., 2016. Tubestone microbialite association in the Ediacaran cap carbonates in the southern Paraguay Fold Belt (SW Brazil): Geobiological and stratigraphic implications for a Marinoan cap carbonate. J. S. Am. Earth Sci. 71, 172–181. https://doi.org/10.1016/J.JSAMES.2016.06.014.
Rothman, D.H., Hayes, J.M., Summons, R.E., 2003. Dynamics of the Neoproterozoic carbon cycle. Proc. Natl. Acad. Sci. U.S.A. 100, 8124–8129. https://doi.org/10.1073/pnas.0832439100.
Sahoo, S.K., Planavsky, N.J., Jiang, G., Kendall, B., Owens, J.D., Wang, X., Shi, X., Anbar, A.D., Lyons, T.W., 2016. Oceanic oxygenation events in the anoxic Ediacaran ocean. Geobiology 14, 457–468. https://doi.org/10.1111/gbi.12182.
Saylor, B.Z., Kaufman, A.J., Grotzinger, J.P., Urban, F., 1998. A composite reference section for terminal Proterozoic strata of southern Namibia. J. Sediment. Res. 68, 1223–1235. https://doi.org/10.2110/JSR.68.1223.
Shields, G., Stille, P., 2001. Diagenetic constraints on the use of cerium anomalies as palaeoseawater redox proxies: an isotopic and REE study of Cambrian phosphorites. Chem. Geol. 175 (1–2), 29–48. https://doi.org/10.1016/S0009-2541(00)00362-4.
Smith, O., 1998. Terminal Proterozoic Carbonate Platform Development: Stratigraphy and Sedimentology of the Kuibis Subgroup (ca. 550–548 Ma). Massachusetts Instit. Technol. (Northern Nama Basin, Namibia).
Spangenberg, J.E., Bagnoud-Velásquez, M., Boggiani, P.C., Gaucher, C., 2014. Redox variations and bioproductivity in the Ediacaran: Evidence from inorganic and organic geochemistry of the Corumbá Group, Brazil. Gondwana Res. 26 (3–4), 1186–1207. https://doi.org/10.1016/j.gr.2013.08.014.
Swart, P.K., Oehlert, A.M., 2018. Revised interpretations of stable C and O patterns in carbonate rocks resulting from meteoric diagenesis. Sediment. Geol. 364, 14–23. https://doi.org/10.1016/J.SEDGEO.2017.12.005.
Tang, J., Johannesson, K., 2010. Ligand extraction of rare earth elements from aquifer sediments: Implications for rare earth element complexation with organic matter in natural waters. Geochem. Cosmochim. Acta 74 (23), 6690–6705. https://doi.org/10.1016/j.gca.2010.08.028.
Tostevin, Rosalie, Shields, G.A., Tarbuck, G.M., He, T., Clarkson, M.O., Wood, R.A., 2016a. Effective use of cerium anomalies as a redox proxy in carbonate-dominated marine settings. Chem. Geol. 438, 146–162. https://doi.org/10.1016/j.chemgeo.2016.06.027.
Tostevin, R., Wood, R.A., Shields, G.A., Poulton, S.W., Guilbaud, R., Bowyer, F., Penny, A.M., He, T., Curtis, A., Hoffmann, K.H., Clarkson, M.O., 2016b. Low-oxygen waters limited habitable space for early animals. Nat. Commun. 7 https://doi.org/10.1038/ncomms12818.
Trompette, R., 1994. Geology of western Gondwana (2000-500 Ma): Pan-African-Brasiliano aggregation of South America and Africa. Geol. Western Gondwana (2000-500 Ma): Pan-African-Brasiliano aggregation of South America and Africa, 00062. https://doi.org/10.1016/0301-9268(95).
Trompette, R., De Alvarenga, C.J.S., Walde, D., 1998. Geological evolution of the Neoproterozoic Corumba graben system (Brazil). Depositional context of the stratified Fe and Mn ores of the Jacadigo Group. J. S. Am. Earth Sci. 11 (6), 587–597. https://doi.org/10.1016/S0895-9811(98)00036-4.
Tucker, M.E., Wright, V.P., 1990. Carbonate Sedimentology. Blackwell Scientific Publications, Oxford, p. 468.
Uhlein, G.J., Uhlein, A., Pereira, E., Caxito, F.A., Okubo, J., Warren, L.V., Sial, A.N., 2019. Ediacaran Paleoenvironmental Changes Recorded in the Mixed Carbonate-Siliciclastic Bambuí Basin. Palaeogeography, Brazil, pp. 39–51. https://doi.org/10.1016/j.palaeo.2018.12.022, 517.
Ullmann, C.V., Korte, C., 2015. Diagenetic alteration in low-Mg calcite from macrofossils: A review. Geological Quarterly. https://doi.org/10.7306/gq.1217.
Veizer, J., 1983. In: Arthur, M.A., Anderson, T.F., Kaplan, I.R., Veizer, J., Land, L.S. (Eds.), Chemical Diagenesis of Carbonates: Theory and Application of Trace Element Technique. https://doi.org/10.2110/scn.83.10.
Walde, D.H.G., Do Carmo, D.A., Guimarães, E.M., Vieira, L.C., Erdtmann, B.D., Sanchez, E.A.M., Adorno, R.R., Tobias, T.C., 2015. New aspects of Neoproterozoic-Cambrian transition in the Corumbá region (state of Mato Grosso do Sul, Brazil). Ann. Palaontol. 101, 213–224. https://doi.org/10.1016/j.annpal.2015.07.002.
Wang, L., Shi, X., Jiang, G., 2012. Pyrite morphology and redox fluctuations recorded in the Ediacaran Doushantuo Formation. Palaeogeography, Palaeoclimatology. Palaeoecology 333–334, 218–227. https://doi.org/10.1016/j.palaeo.2012.03.033.
Wang, P., Yongjian, H., Chengshan, W., Sihui, F., Qinghua, H., 2013. Pyrite morphology in the first member of the Late Cretaceous Qingshankou Formation, Songliao Basin, Northeast China. Palaeogeography, Palaeoclimatology. Palaeoecology 385, 125–136. https://doi.org/10.1016/j.palaeo.2012.09.027.
Warren, L.V., Quaglio, F., Simões, M.G., Gaucher, C., Riccomini, C., Poiré, D.G., Freitas, B.T., Boggiani, P.C., Sial, A.N., 2017. Cloudina-Corumbella-Namacalathus association from the Itapucumi Group, Paraguay: Increasing ecosystem complexity and tiering at the end of the Ediacaran. Precambrian Res. 298, 79–87. https://doi.org/10.1016/J.PRECAMRES.2017.05.003.
Wilkin, R.T., Barnes, H.L., Brantley, S.L., 1996. The size distribution of framboidal pyrite in modern sediments: An indicator of redox conditions. Geochem. Cosmochim. Acta 60 (20), 3897–3912. https://doi.org/10.1016/0016-7037(96)00209-8.
Wood, R., Liu, A.G., Bowyer, F., Wilby, P.R., Dunn, F.S., Kenchington, C.G., Cuthill, J.F. H., Mitchell, E.G., Penny, A., 2019. Integrated records of environmental change and evolution challenge the Cambrian Explosion. Nat. Ecol. Evol. 3, 528–538. https://doi.org/10.1038/s41559-019-0821-6.
Wood, R.A., Poulton, S.W., Prave, A.R., Hoffmann, K.H., Clarkson, M.O., Guilbaud, R., Lyne, J.W., Tostevin, R., Bowyer, F., Penny, A.M., Curtis, A., Kasemann, S.A., 2015. Dynamic redox conditions control late Ediacaran metazoan ecosystems in the Nama Group, Namibia. Precambrian Res. 261, 252–271. https://doi.org/10.1016/J.PRECAMRES.2015.02.004.
Yang, C., Rooney, A.D., Condon, D.J., Li, X.H., Grazhdankin, D.V., Bowyer, F.T., Hu, C., Macdonald, F.A., Zhu, M., 2021. The tempo of Ediacaran evolution. Sci. Adv. 7, 1–11. https://doi.org/10.1126/sciadv.abi9643.
Zaine, M.F., 1991. Análise dos fósseis de parte da Faixa Paraguai (MS, MT) e seu contexto temporal e paleoambiental. Universidade de São Paulo, São Paulo, Brazil. PhD Thesis.
Zaine, M.F., Fairchild, T.R., 1985. Comparison of Aulophycus lucianoi Beurlen & Sommer from Ladário (MS) and the genus Cloudina Germs, Ediacaran of Namibia. An Acad. Bras Ciências 57 (1), 130.
Zaine, M.F., Fairchild, T.R., 1987. Novas considerações sobre os fósseis da Formação Tamengo, Grupo Corumbá, SW do Brasil. Anais do Congresso Brasileiro de Paleontologia 10, 797–807, 1987, Rio de Janeiro.
Zhang, J., Nozaki, Y., 1996. Rare earth elements and yttrium in seawater: ICP-MS determinations in the East Caroline, Coral Sea, and South Fiji basins of the western South Pacific Ocean. Geochem. Cosmochim. Acta 60, 4631–4644. https://doi.org/10.1016/S0016-7037(96)00276-1.
Zhang, K., Zhu, X., Yan, B., 2015. A refined dissolution method for rare earth element studies of bulk carbonate rocks. Chem. Geol. 412, 82–91. https://doi.org/10.1016/j.chemgeo.2015.07.027.
Zhao, Y., Wei, W., Santosh, M., Hu, J., Wei, H., Yang, J., Liu, S., Zhang, G., Yang, D., Li, S., 2022. A review of retrieving pristine rare earth element signatures from carbonates. Palaeogeography, Palaeoclimatology,. Palaeoecology 586, 110765. https://doi.org/10.1016/j.palaeo.2021.110765.
Zhao, Y., Wei, W., Li, S., Yang, T., Zhang, R., Somerville, I., Santosh, M., Wei, H., Wu, J., Yang, J., Chen, W., Tang, Z., 2021. Rare earth element geochemistry of carbonates as a proxy for deep-time environmental reconstruction. Palaeogeography,

Palaeoclimatology. Palaeoecology 574, 110443. https://doi.org/10.1016/j.palaeo.2021.110443.

Zhu, M., Babcock, L.E., Peng, S., 2006. Advances in Cambrian stratigraphy and paleontology: Integrating correlation techniques, paleobiology, taphonomy and paleoenvironmental reconstruction. Paléo 14 (3–4), 217–222. https://doi.org/10.1016/j.palwor.2006.10.016.

Zhu, M., Zhuravlev, A.Y., Wood, R.A., Zhao, F., Sukhov, S.S., 2017. A deep root for the Cambrian explosion: Implications of new bio and chemostratigraphy from the Siberian Platform. Geology 45. https://doi.org/10.1130/G38865.1.